

Lewis Structures and the Bonding Classification of End-on Bridging Dinitrogen Transition Metal Complexes

Faraj Hasanayn,* Patrick L. Holland, Alan S. Goldman, and Alexander J. M. Miller*



Cite This: *J. Am. Chem. Soc.* 2023, 145, 4326–4342



Read Online

ACCESS |



Metrics & More



Article Recommendations



Supporting Information

ABSTRACT: The activation of dinitrogen by coordination to transition metal ions is a widely used and promising approach to the utilization of Earth's most abundant nitrogen source for chemical synthesis. End-on bridging N_2 complexes ($\mu\text{-}\eta^1\text{:}\eta^1\text{-}N_2$) are key species in nitrogen fixation chemistry, but a lack of consensus on the seemingly simple task of assigning a Lewis structure for such complexes has prevented application of valence electron counting and other tools for understanding and predicting reactivity trends. The Lewis structures of bridging N_2 complexes have traditionally been determined by comparing the experimentally observed NN distance to the bond lengths of free N_2 , diazene, and hydrazine. We introduce an alternative approach here and argue that the Lewis structure should be assigned based on the total π -bond order in the MNNM core (number of π -bonds), which derives from the character (bonding or antibonding) and occupancy of the delocalized π -symmetry molecular orbitals (π -MOs) in MNNM. To illustrate this approach, the complexes *cis,cis*-[(^{iPr}4PONOP)MCl₂]₂($\mu\text{-}N_2$) (M = W, Re, and Os) are examined in detail. Each complex is shown to have a different number of nitrogen–nitrogen and metal–nitrogen π -bonds, indicated as, respectively: $W\equiv N\text{--}N\equiv W$, $Re=N=N=Re$, and $Os\text{--}N\equiv N\text{--}Os$. It follows that each of these Lewis structures represents a distinct class of complexes (diazanyl, diazenyl, and dinitrogen, respectively), in which the $\mu\text{-}N_2$ ligand has a different electron donor number (total of $8e^-$, $6e^-$, or $4e^-$, respectively). We show how this classification can greatly aid in understanding and predicting the properties and reactivity patterns of $\mu\text{-}N_2$ complexes.

INTRODUCTION

Dinitrogen would be an ideal resource in chemical synthesis since it makes up roughly 80% of the Earth's atmosphere, but this abundant feedstock is resistant to activation and functionalization. The only large-scale industrial reaction of N_2 commercialized to date is the Haber–Bosch process for ammonia synthesis. While revolutionary in its time,¹ the Haber–Bosch process employs harsh conditions and relies on hydrogen from fossil fuels, leading to unsustainable levels of CO₂ emissions. With the demands for ammonia continuing to rise, developing a more sustainable synthesis from N_2 has become an urgent goal.^{2–6}

Chemists working toward N_2 functionalization under mild conditions have been guided by the hypothesis that binding N_2 to a transition metal ion can activate it toward synthetic modification.⁷ Numerous metal– N_2 complexes spanning the periodic table have been prepared, and reactivity of the bound N_2 ligand has been demonstrated, including catalytic examples of ammonia and hydrazine formation among other reactions.^{8–12}

One key factor influencing the prospects and mechanism of functionalization is the N_2 binding mode,¹³ with end-on terminal (η^1) and end-on bridging ($\mu\text{-}\eta^1\text{:}\eta^1\text{-}N_2$, which we simplify to $\mu\text{-}N_2$ herein) modes most commonly observed. Although it has historically been difficult to predict which mode will be adopted, we recently showed that an MO-based analysis considering the number of d-electrons supplied by the two metals to the π -MNNM manifold can correctly predict the

preference for end-on terminal or bridged coordination (eq 1).¹⁴



Side-on bridging N_2 coordination is also known, with the nature of the metal and steric factors proposed to be responsible for controlling which bridging mode is adopted;^{15–19} however, we focus on end-on binding here.

The common view of bonding (and Lewis structure representation) in dinitrogen complexes has been shaped by the synergy model of ligand-to-metal σ -donation and metal-to-ligand π -backdonation,^{20–22} akin to that used for metal–CO bonding²³ and the original Dewar–Chatt–Duncanson model for η^2 -olefin coordination.^{24,25} Within this model, the degree of π -backbonding upon N_2 coordination is gauged based on changes in the bond lengths (r_{NN}) and stretching vibrational frequencies (ν_{NN}). For N_2 binding to a single metal in an end-on mode, crystal structures reveal only minor effects on r_{NN} , and IR spectroscopy shows similarly small effects on ν_{NN} , with the lowest ν_{NN} values reaching around 1910 cm^{-1} .^{26–29} The Lewis structure for terminal MN_2 complexes is therefore generally drawn with a single M–N bond and a triple $N\equiv N$

Published: February 16, 2023



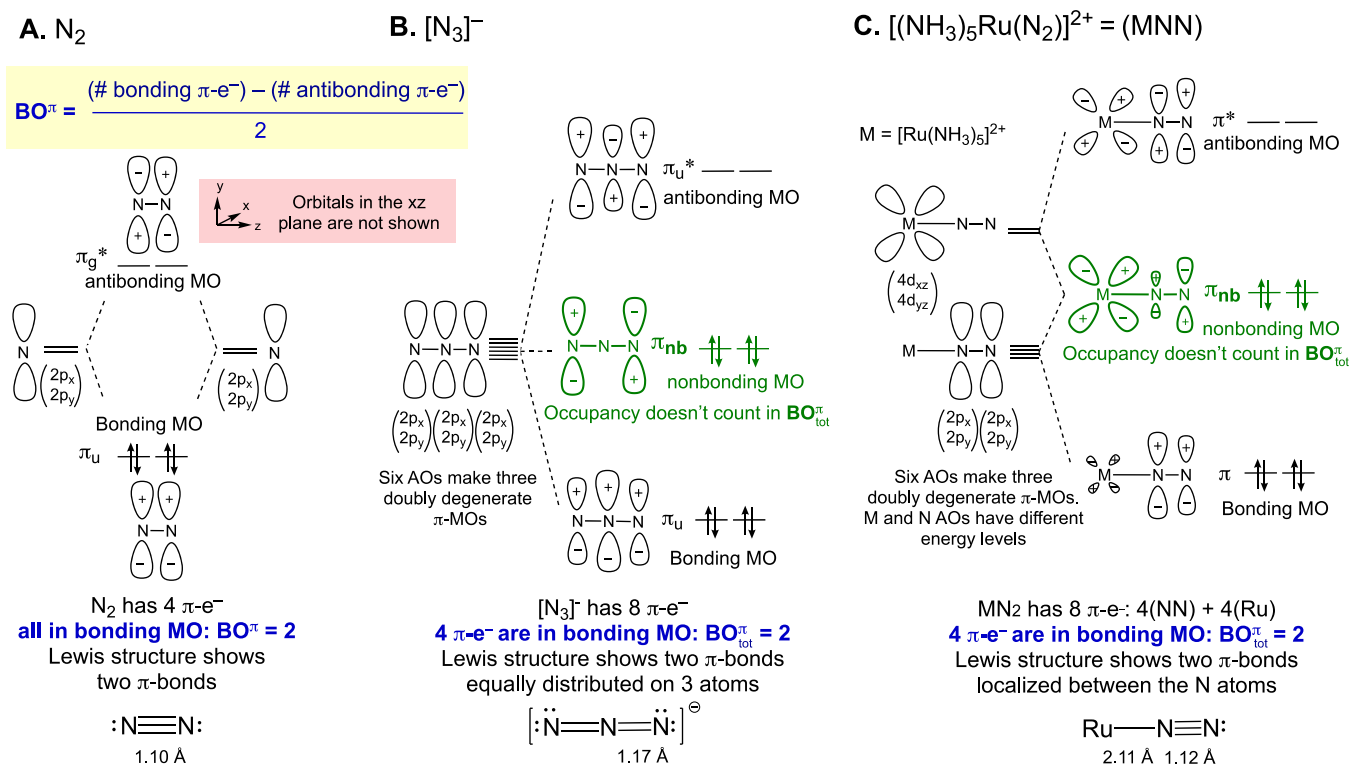


Figure 2. π -MO diagrams and Lewis structures for N_2 , $[N_3]^-$, and $[(NH_3)_5Ru(N_2)]^{2+}$. Only one of each pair of doubly degenerate π -MOs is drawn.

starting from simple examples in order to clarify how our model for metal- N_2 complexes is analogous to these well-accepted molecules.

To orient readers with the “ π -only” MO diagrams, we first illustrate the diatomic ligand of interest, N_2 (Figure 2A). The $(2p_x, 2p_y)$ AOs of nitrogen are suitable for π -bonding in N_2 , generating a basis set of four AOs. The in-phase combinations of the AOs (constructive interference) create a doubly degenerate bonding π -MO (π_u) with an energy level lower than that of the AOs. The out-of-phase AO combinations (destructive interference) generate a doubly degenerate antibonding π -MO (π_g^*) with a node between the atoms and an energy higher than that of the AOs. MO diagrams are used to define a π -bond order (BO^π) as half the difference between the number of electrons in the bonding and antibonding π -MOs (Figure 2A).⁴⁰ For N_2 , each atom provides two electrons to the π -MOs; in the ground state, four electrons fill the low energy bonding π -MO, so $BO^\pi = 2$. This is equivalent to the number of π -bonds in the Lewis structure of N_2 .

Next, we consider π -bonding in the azide ion $[N_3]^-$ (Figure 2B). In the linear geometry, three pairs of $(2p_x, 2p_y)$ AOs are transformed into three delocalized doubly degenerate π -MOs. Estimates of the AO coefficients and relative energies of the π -MOs can be obtained using the Hückel MO method.⁴¹ In this Perspective we are concerned primarily with the total bond order in linear moieties (BO^π_{tot}). As shown in Figure 2B, the AO interactions in $[N_3]^-$ afford three π -MOs: one bonding (π_u), one nonbonding (π_{nb}), and one antibonding (π_u^*). The characters of these MOs are related to those of the familiar allyl anion and CO_2 , and can be easily obtained by dividing $[N_3]^-$ into two fragments and considering their interactions (Figure SI-1A).³⁹ $[N_3]^-$ has 8 π -electrons; four fill π_u and four fill π_{nb} ,

resulting in $BO^\pi_{\text{tot}} = 2$. Because the terminal atoms are identical, each NN linkage has a “local” NN $BO^\pi = 1$. This matches the Lewis structure drawn for $[N_3]^-$ based on localized shared electron pairs.

Figure 2C considers π -bonding in the terminal RuNN bond of $[(NH_3)_5Ru(N_2)]^{2+}$, the first reported dinitrogen complex.^{42–44} As in $[N_3]^-$, the $(2p_x, 2p_y)$ AOs of nitrogen and the $(4d_{xz}, 4d_{yz})$ AOs of Ru are expected to generate three doubly degenerate π -MOs in RuNN. Because the Ru and N AOs have different energy levels, the coefficients from Ru and N will be different in the MOs. In analogy to an ethylene molecule substituted with a π -donor orbital having an energy level higher than the bonding π -MO of ethylene,⁴⁵ we expect the lowest energy π -MO in RuNN to be concentrated on NN, and the second π -MO to have principal coefficients from Ru and the distal nitrogen (Figure SI-2A). Such a nonbonding view of the second π -MO in the MNN bond was adopted by DuBois and Hoffmann to describe the electron density distribution in MNN complexes.⁴⁶

The square pyramidal fragment $[(NH_3)_5Ru]^{2+}$ has a d^6 - Ru^{II} center that provides 4 electrons for π -bonding in RuNN. N_2 provides 4 additional electrons leading to a $(\pi)^4(\pi_{\text{nb}})^4$ configuration. The BO^π_{tot} in RuNN is therefore 2, similar to $[N_3]^-$. However, because the bonding π -MO is concentrated on the nitrogen atoms, a Lewis representation of the MO-based BO^π_{tot} would localize both π -bonds between the nitrogen atoms, $\text{Ru}-\text{N}\equiv\text{N}$. The given π -bonding picture in MNN implicates a constant $BO^\pi_{\text{tot}} = 2$ independent of the occupancy of π_{nb} and can explain why the NN bond distance of terminal MN_2 complexes is generally not highly sensitive to the metal. This is fundamentally different from bridging N_2 complexes, as we will show in the subsequent sections.

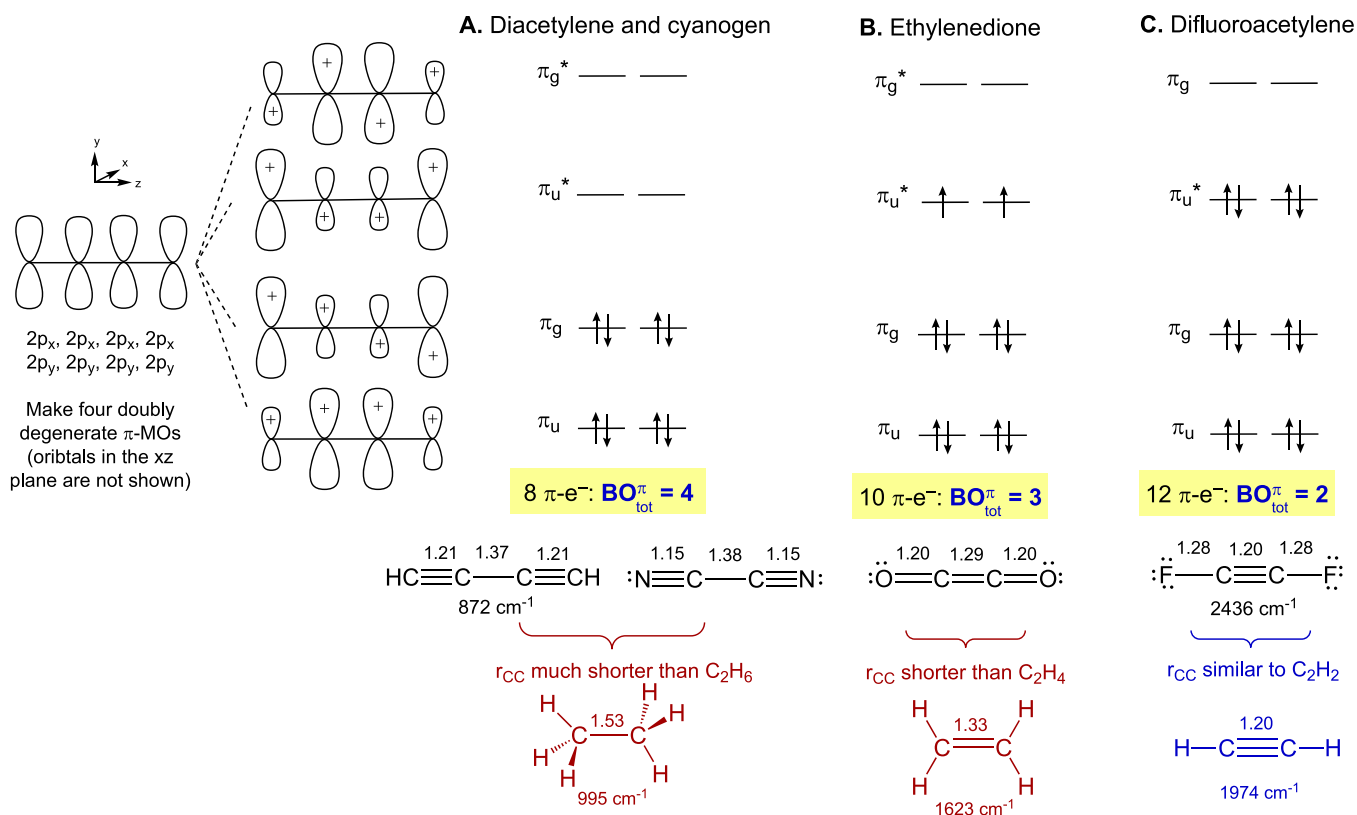


Figure 3. π -MO diagrams and Lewis structures for some linear tetratomic organic molecules. Bond distances in Å. For clarity, only one of each pair of doubly degenerate π -MOs is drawn.

■ π -MO DIAGRAMS AND LEWIS STRUCTURES OF ORGANIC MOLECULES WITH LINEAR TETRATOMIC CORES

Delocalized π -bonding in organic systems is a classic test of MO theory. We sought similarly simple systems with tetratomic cores that could serve as conceptual “bridges” between familiar organic molecules and transition metal μ - N_2 complexes.³⁶

We start in Figure 3 with butadiyne (diacetylene), which has a linear tetratomic core appropriate for building isolobal analogies with the linear MNNM cores of bridging N_2 complexes. The eight ($2p_x, 2p_y$) AOs of the carbons transform into four doubly degenerate delocalized π -MOs, two bonding (π_u and π_g) and two antibonding (π_u^* and π_g^*). Again, the shape of the MOs can be constructed using the fragment approach (Figure SI-1B), and the AO coefficients can be quantified using the Hückel MO method,^{38,41} or a recently reported graphical method.⁴⁷

Each carbon in diacetylene provides two electrons to the π -system. The total of 8 electrons fills the bonding π_u and π_g , leading to a closed shell singlet state with a total of four π -bonds ($BO_{\text{tot}}^{\pi} = 4$; Figure 3A). Experimentally, the terminal CC bonds in diacetylene are much shorter than the central CC bond, 1.21 versus 1.37 Å.^{48,49} MO theory attributes this difference to the presence of a node in π_g that imparts antibonding character selectively to the central CC segment of the MO, thereby removing the “local” π -bond from between the two atoms acquired from the filling of π_u .⁵⁰ This effect is well captured in the familiar Lewis structure of diacetylene, $\text{HC}\equiv\text{C}-\text{C}\equiv\text{CH}$. Consistent with this representation, the bond length of the terminal CC bonds in diacetylene is similar

to the C–C bond length in acetylene: 1.21 and 1.20 Å, respectively.⁵¹ However, although the central carbons in diacetylene, butadiene, and *n*-butane are each represented as being connected by a single σ -bond, the bond length varies considerably among the three molecules: 1.37, 1.47, and 1.53 Å, respectively.⁵¹ A commonly adopted explanation for these variations is hybridization, with the increased *s*-character in the C–C bond drawing the atoms closer.^{38,52,53} While the detailed contributors to the observed variations can still be a subject of debate,^{54–58} all chemists accept that diacetylene is best represented using a Lewis structure with a central single bond, even though the bond distance is closer to ethylene than it is to ethane (Figure 3). It therefore becomes clear that any bond distance comparisons should take into account whether the bonding picture is similar between the molecules being compared or not.

The MO π -bonding picture in diacetylene is equally applicable to the linear tetratomic species cyanogen, NCCN , which also has 8 π -electrons. The same Lewis structure, $\text{N}\equiv\text{C}-\text{C}\equiv\text{N}$, is therefore adopted. Consistently, the CC bond length of cyanogen and the central CC bond in diacetylene are similar.⁵⁹ Note that even though the atoms in cyanogen are not identical, contrasting with the case of the diacetylene core, the π -MOs maintain the same character and phasing; only the orbital coefficients are perturbed due to differences in the electronegativity of the heteroatoms (Figure SI-3). From cyanogen, one can envision a series varying the terminal atoms while moving across the period, from NCCN to OCCO to FCCF . If one considered the CC group a bridge between the terminal atoms, this would be analogous to changing the metal atoms in a MNNM core.

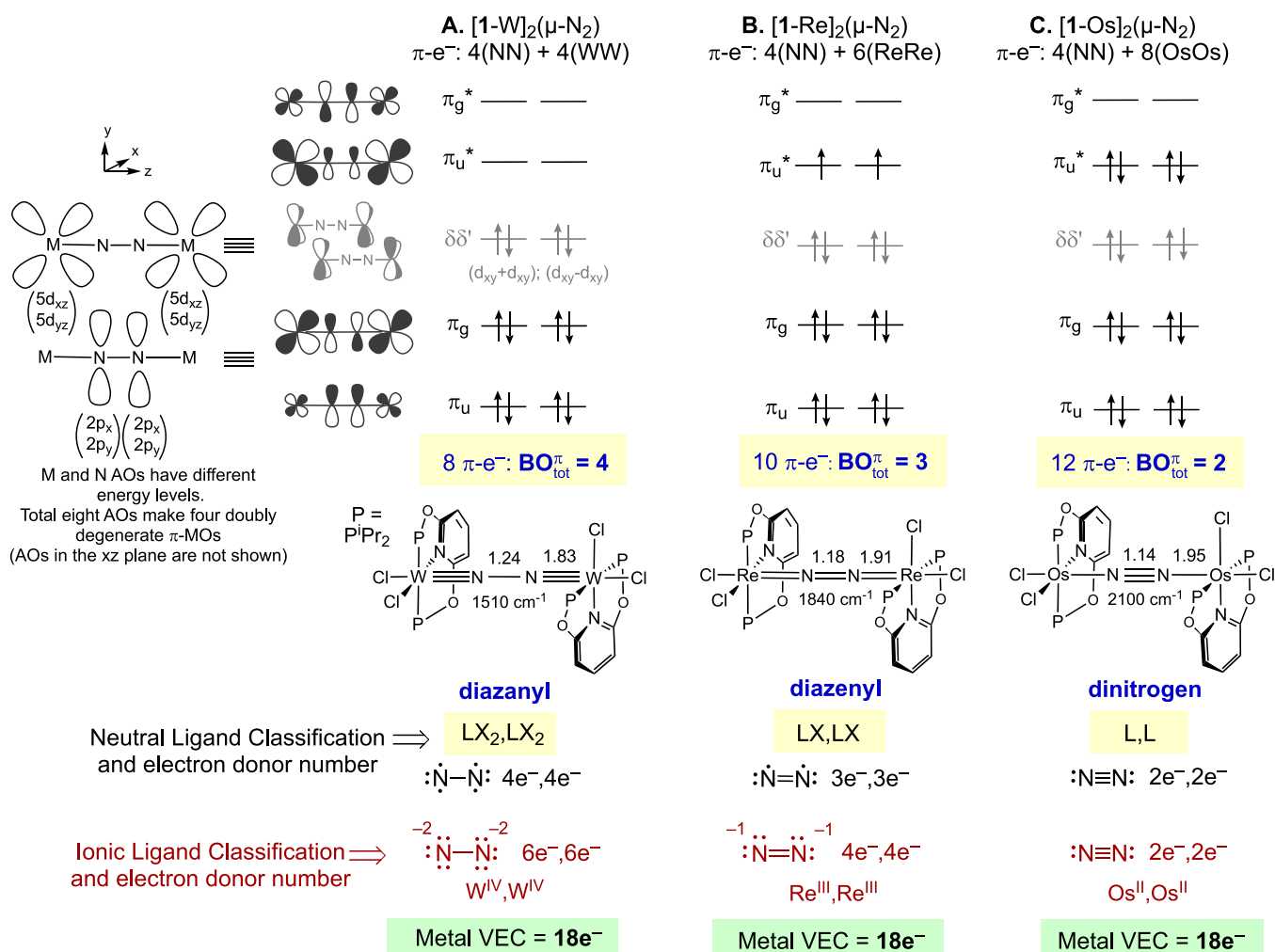


Figure 4. π-MO diagrams, Lewis structures, and Valence Electron Count in [1-M]₂(μ-N₂) (M = W, Re, and Os). For clarity, only one of each pair of π-MOs is drawn. Note that [1-M]₂(μ-N₂) has a C₂ point group, but in the pseudo-D_{4h} geometry the π-MOs (with a and b symmetries) remain essentially degenerate (Figure SI-2). Bond distances in Å.

The carbon and oxygen (2p_x, 2p_y) AOs in ethylenedione, OCCO, transform into delocalized π-MOs as in diacetylene and cyanogen, but there are now 2 additional electrons in the π-manifold (a total of 10 π-e⁻), so OCCO has a (π_u)⁴(π_g)⁴(π_u^{*})² configuration.⁶⁰ The partial occupancy of π_u^{*} lowers the total bond order BO_{tot}^π to 3. Since π_u^{*} has a π-node in each of the terminal CO bonds but not in CC, the local π-bonding character in the CC bond is increased compared to the CC bond in cyanogen, and this is clearly manifested in a significantly shorter CC bond length compared to NCCN, 1.29 versus 1.38 Å. Based on the position of the nodes in the MOs, we arrive at a Lewis structure of O=C=C=O for this molecule.

The use of two parallel arrows in the MO diagram in Figure 3B implies a triplet spin state, but the partial occupancy of π_u^{*} actually produces three electronic states: a triplet ³Σ_g⁻, a doubly degenerate closed shell singlet ¹Δ_g, and an open shell singlet ¹Σ_g⁺. From *ab initio* calculations, the ³Σ_g⁻ state is found to be the ground state, with ¹Δ_g and ¹Σ_g⁺ higher in energy by 6.9 and 9.5 kcal/mol, respectively.⁶⁰ These states are all computed to have comparable CC bond lengths,⁶⁰ which is expected because they arise from the same MO occupancy, implying BO_{tot}^π is the same. Note that even though there are two unpaired electrons in the ground state, Lewis structures

avoid the use of dashed lines of the types often drawn in analogous MNNM cores.

Lastly, Figure 3C considers difluoroacetylene, FCCF. With 12 electrons in π-symmetry orbitals, the (π_u)⁴(π_g)⁴(π_u^{*})⁴ configuration gives a closed shell singlet state with BO_{tot}^π = 2. By the same reasoning based on the position of the nodes followed above, the full occupancy of π_u^{*} localizes the two π-bonds in between the central carbons. Consistently, FCCF has a shorter CC bond (1.20 Å) than ethylenedione (1.29 Å) and cyanogen (1.38 Å).⁶¹ The familiar Lewis structure F-C≡C-F accurately captures the electronic and structural features inferred from the π-MOs. Expectedly, the frequency of the CC stretching vibrational mode (ν_{CC}) in FCCF (2436 cm⁻¹; Figure 3C) is much higher than that of the C₂-C₃ stretching mode of diacetylene (872 cm⁻¹; Figure 3A).

The outcome of Figure 3 is a direct connection between the number and position of bonds in Lewis structures and the total bond order and position of the nodes from MO theory. For such organic molecules the Lewis structures are readily drawn without inspection of an MO diagram. But it is clear that assigning Lewis structures for NCCN and OCCO using the CC bond distances or stretch frequencies of ethane and ethylene as reference would not work. This must raise doubts about using diatomic N₂, N₂H₂, and N₂H₄ for comparisons to

complexes with tetratomic MNNM cores. Drawing Lewis structures directly for multinuclear transition metal complexes can be more challenging, but the task is greatly simplified when one starts with qualitative MO diagrams as we demonstrate in the following section.

MO-DERIVED LEWIS STRUCTURES OF μ -N₂ COMPLEXES

The π -MO diagrams of the MNNM core of μ -N₂ complexes can be constructed and analyzed in a fashion analogous to the organic molecules described above in order to inform the systematic drawing of Lewis structures. Figure 4 illustrates the different bonding situations in a series of end-on bridging N₂ complexes having identical ligands and geometries, *cis,cis*-[(^{iPr}4PONOP)MCl₂]₂(μ -N₂), [1-M]₂(μ -N₂) (M = W, Re, and Os).³⁷

The metals in the given series use the (5d_{xz},5d_{yz}) AOs for π -interaction with the (2p_{xy},2p_y) AOs of nitrogen, forming two bonding MOs, π_u and π_g , and two antibonding MOs, π_u^* and π_g^* , having the same phases (number and position of the nodes) as in the organic tetratomic molecules. The nonbonding 5d_{xy} AOs on the two metals transform into a pair of MOs corresponding to their in-phase (d_{xy}+d_{xy}) and out-of-phase (d_{xy}-d_{xy}) symmetry adapted linear combinations, and are labeled as $\delta\delta'$ to specify they are orthogonal to the MNNM axis. As noted for cyanogen, the AO coefficients are expected to vary in the different π -MOs of MNNM because nitrogen is more electronegative than M, but this does not alter the bonding/antibonding assignments of the MOs that lead to the calculation of BO_{tot} ^{π} . As we demonstrate in subsequent sections, the π -MO diagram derived in Figure 4 is readily adapted to other geometries in which each metal has two d-AOs with π -symmetry in the MNNM core, but a modified diagram is needed in certain cases such as metallocenes where each metal provides only one d-AO with π -symmetry to the MNNM core.

The two nitrogen atoms provide four electrons to the π -MOs of all μ -N₂ complexes, so the lowest-energy doubly degenerate MO π_u is always filled. The occupancy of π_g , $\delta\delta'$, and π_u^* , on the other hand, varies depending on the metal. The fragment [(^{iPr}4PONOP)WCl₂] ([1-W]) has a d⁴-W^{II} center. When two d⁴-[1-W] metals are bridged with N₂, four electrons fill the bonding MO π_g of WNNW and four electrons fill the nonbonding $\delta\delta'$. The resulting (π_u)⁴(π_g)⁴ π -configuration creates BO_{tot} ^{π} = 4 in WNNW. Because π_g has a node between the N atoms, the bridge is a diazanyl group with the matching Lewis structure of W≡N–N≡W, analogous to diacetylene and cyanogen. Octahedral W and Nb μ -N₂ complexes with (π_u)⁴(π_g)⁴ configurations are known, and have previously been assigned M≡N=N≡M or M=N–N=M Lewis structures based on the crystallographic NN bond length (r_{NN} = 1.22–1.28 Å) and the method outlined in Figure 1A.^{62,63} These examples illustrate how the empirical and the MO-based Lewis structures can often differ: the MO-based Lewis structures would all be assigned M≡N–N≡M. The computed r_{NN} in [1-W]₂(μ -N₂) is 1.24 Å, similar to the experimentally studied complexes—but far shorter than r_{NN} in hydrazine (1.45 Å). We have seen earlier, however, how diacetylene and cyanogen exhibit short C–C bonds that are still best represented as single bonds in Lewis structures. Similarly, comparisons to hydrazine are not helpful in calibrating structural representations in MNNM.

Next, Figure 4B illustrates the dirhenium complex [1-Re]₂(μ -N₂). The MNNM core now has 10 π -electrons in a

(π_u)⁴(π_g)⁴(π_u^*)² configuration leading to BO_{tot} ^{π} = 3. Just as with ethylenedione, the partial occupancy of π_u^* gives rise to three different electronic states. DFT calculations predict [1-Re]₂(μ -N₂) to have a triplet spin ground state, and put the open and closed shell singlet states at 9.4 and 11.4 kcal/mol, respectively.³⁷ Experimentally, solutions of [1-Re]₂(μ -N₂) exhibit spectroscopic signatures consistent with temperature-independent paramagnetism (TIP).³⁷ Because π_u^* has nodes between the M and N atoms and no node between the N atoms, the bridge is a diazenyl group with the matching Lewis structure of Re=N=N=Re, with two fewer MN π -bonds and one more NN π -bond compared to [1-W]₂(μ -N₂). The ReNNRe core in [1-Re]₂(μ -N₂) is isolobal to ethylenedione and thus adopts an analogous Lewis structure. Finally, in the diosmium complex [1-Os]₂(μ -N₂) shown in Figure 4C there are 12 π -electrons in a (π_u)⁴(π_g)⁴(π_u^*)⁴ configuration leading to BO_{tot} ^{π} = 2 and an Os–N≡N–Os Lewis structure that is analogous to difluoroacetylene, F–C≡C–F.

The trends in the computed r_{MN} and r_{NN} in the three complexes in Figure 4 are consistent with the MO-derived local MN and NN BO ^{π} assignments. Thus, in moving from W to Re to Os: (a) there are fewer MN π -bonds, and r_{MN} increases uniformly from 1.83 Å (W≡N) to 1.91 Å (Re=N) and to 1.95 Å (Os–N); (b) there are more NN π -bonds, and r_{NN} decreases from 1.24 Å (WN–NW) to 1.18 Å (ReN=NRe) and to 1.14 Å (OsN≡NOs) while concomitantly ν_{NN} increases from 1510 to 1840 and to 2100 cm⁻¹.¹⁹ In contrast, focusing only on metal-to-ligand backbonding could have led one to predict the opposite trends in r_{NN} and ν_{NN} , since one might have expected increased backbonding, shorter r_{NN} , and lower ν_{NN} for the metals that have more π -electrons. The small magnitudes of the changes in r_{NN} for the varied local NN BO ^{π} in Figure 4 are in line with the small changes in r_{CC} for the linear organic molecules in Figure 3. As we now would expect based on the organic molecules introduced above, the N–N distances in linear N₂-bridged complexes are not expected to approach the N–N distance of hydrazine (1.45 Å, Figure 1).

VALENCE ELECTRON COUNT (VEC) AND THE 18e⁻ RULE

With the availability of the MO-based Lewis structures, we can now determine the valence electron count (VEC) on each metal of μ -N₂ complexes. In Figure 4 we show the electron donor type of a bridging N₂ in each of the different Lewis structures using both the covalent bond classification (CBC) approach (neutral ligand formalism),^{64–66} and the ionic ligand formalism.

In CBC, μ -N₂ is removed from each complex as a neutral ligand preserving the number of NN π -bonds in a given Lewis structure. In all cases, each end of the NN bridge acts as an L-type 2e⁻ σ -donor ligand to one metal. Each unpaired electron left on a given N acts as an additional X-type 1e⁻ π -donor to one metal. In the ionic model, on the other hand, enough electrons are added to μ -N₂ so that each MN π -bond in the Lewis structure is formed by a 2e⁻ dative N to M bond. In [1-W]₂(μ -N₂), the Lewis structure is W≡N–N≡W, so the neutral NN bridge acts as an LX₂LX₂ ligand, donating two σ -electrons and two π -electrons (total 4 electrons) to each metal. In [1-Re]₂(μ -N₂), the Lewis structure is Re=N=N=Re and μ -N₂ acts as an LX₂LX ligand, donating 3 electrons to each metal. Finally, for [1-Os]₂(μ -N₂), there are no MN π -bonds, so μ -N₂ is an L-type 2e⁻ σ -donor to each metal.

Using the ionic model, the bridging NN in $[1-W]_2(\mu-N_2)$, $[1-Re]_2(\mu-N_2)$, and $[1-Os]_2(\mu-N_2)$ would correspond to hydrazine-tetraide ($[N_2]^{4-}$), diazene-diide ($[N_2]^{2-}$), and dinitrogen (N_2) respectively, and the metals would have varied formal oxidation states: W^{IV} , Re^{III} , and Os^{II} . Strikingly, therefore, the MO-based analysis leads to Lewis structures in which the bridging N_2 ligand alters its donor number depending on the metal, leading thereby to a constant VEC = $18e^-$ across the series. Note that any Lewis structure other than the one used for each specific complex in Figure 4 would have resulted in a VEC $\neq 18e^-$. Only with a systematically applied Lewis structure can a meaningful valence electron count be performed. The variable electron donor properties of the N_2 bridge have similarities to other ligands such as the terminal nitrosyl and oxo ligands.^{65,66}

Establishing that the complexes in Figure 4 have filled valences (i.e., having 18 valence electrons) reveals some interesting similarities to the organic molecules discussed in Figure 4 as well as to the diatomic molecules N_2 , O_2 , and F_2 . In particular, $[1-Re]_2(\mu-N_2)$ is a persistent diradical with a full valence shell, similar to that encountered in O_2 and ethylenedione. Linear tetratomic organic molecules with 10 π -electrons have been of great interest but proved to be challenging to make or even detect. Ethylenedione, for example, is predicted to be intrinsically unstable toward dissociation into two CO molecules,⁶⁷ and has never been experimentally detected, while the isoelectronic ethylenedithione SCCS can be prepared and characterized only at low pressures.⁶⁸ $[1-Re]_2(\mu-N_2)$ therefore provides a striking example of an isolable system with 10 π -electrons in a linear tetratomic core. Other examples of isolable and crystallographically determined 10 π - e^- $\mu-N_2$ complexes are given in Scheme 1, including two that undergo facile (*below* room temperature) cleavage into two terminal nitrides, a reaction of immense current interest in the chemistry of N_2 functionalization.^{32,69}

As shown in Scheme 1, various Lewis structures have been reported for the isolated 10 π - e^- complexes, typically using dashed lines. But the MO-derived method assigns the same Lewis structures for all of these, namely $M=N=N=M$. Once we recognize that this family of N_2 -splitting complexes all have the same Lewis structures, we can start to see how the three distinct Lewis structures with varied numbers of π -bonds correlate with distinct reactivity patterns, which we follow up on in the following sections.

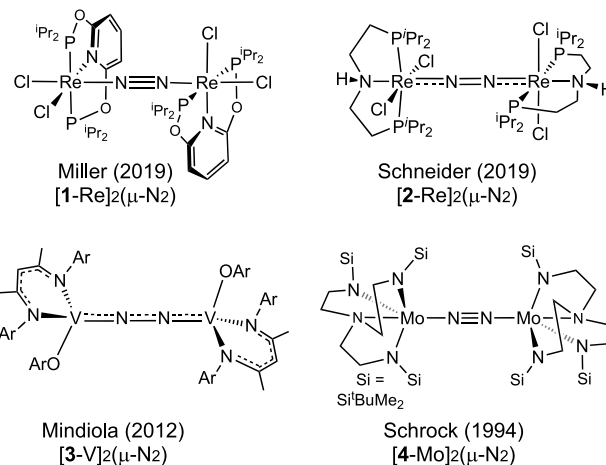
LEWIS STRUCTURE AND THE REACTIONS OF $[1-M]_2(\mu-N_2)$ WITH N_2 AND H_2

To illustrate how categorizing bridging N_2 complexes based on the MO-derived Lewis structures can aid in predicting thermodynamic trends we consider in Figure 5 the reaction between $[1-M]_2(\mu-N_2)$ and N_2 to give two octahedral terminal MN_2 products (L_3M-N_2). In the given reaction, the number of σ -bonds is the same in the reactants and the products, so we can limit our analysis to the π -bonds.

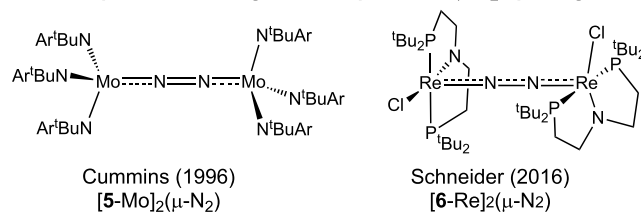
As discussed in Figure 2, the terminal MNN moiety in the product has a fixed $BO_{tot}^{\pi} = 2$ regardless of the number of d_{π} electrons provided by the metal, and thus the Lewis structure is uniformly represented as $M-N\equiv N$. The BO^{π} in the free N_2 molecule is also 2. Because BO_{tot}^{π} in the MNNM core of $[1-M]_2(\mu-N_2)$ varies, the transformation from bridging to terminal coordination is associated with a change in the total number of π -bonds (ΔBO_{tot}^{π}) that varies depending on the

Scheme 1. Representative Isolable $\mu-N_2$ Complexes Having 10 π - e^- $M=N=N=M$ Cores^a

A. Examples that do not undergo thermal $\mu-N_2$ splitting



B. Examples that undergo low temp thermal $\mu-N_2$ splitting



^aLewis structures are given as originally reported in the literature.

metal. The diazanyl complex $[1-W]_2(\mu-N_2)$ has $BO_{tot}^{\pi} = 4$; when it reacts with N_2 to form two terminal N_2 complexes, two π -bonds are lost ($\Delta BO_{tot}^{\pi} = -2$) so the reaction is expected to be highly unfavorable. The analogous reaction of the diazenyl complex $[1-Re]_2(\mu-N_2)$ results in the loss of only one π -bond ($\Delta BO_{tot}^{\pi} = -1$), and it too is expected to be disfavored, but not as much as when $\Delta BO_{tot}^{\pi} = -2$. In contrast, in the reaction of $[1-Os]_2(\mu-N_2)$ with N_2 no bonds are gained or lost ($\Delta BO_{tot}^{\pi} = 0$), so the reaction is expected to be nearly ergoneutral. In the latter case, attractive dispersion interactions can play a role in favoring bridge formation.^{70,71} The computed free energies included in Figure 5 strongly support the qualitative conclusions based on ΔBO_{tot}^{π} .¹⁴

Another way to use the Lewis structures to explain the reaction energy trends in Figure 5 is to compare the VECs in the reactants and products. Regardless of the initial donor number, when the N_2 ligand converts from bridging to terminal coordination it becomes a simple $2e^-$ L type ligand. Note that N_2 is a $2e^-$ donor even in the limiting $M=N=N$ Lewis structure of a terminal $M-NN$ bond, acting as an X_2 type ligand. As such, the different classes of bridging $18e^-$ complexes yield terminal MNN complexes having variable VECs. One anticipates that the bridging complexes with two $18e^-$ metal centers, $[1-W]_2(\mu-N_2)$ or $[1-Re]_2(\mu-N_2)$, should be favored over the corresponding monometallic terminal N_2 complexes that have VECs of $16e^-$ and $17e^-$, respectively. On the other hand, $[1-Os]_2(\mu-N_2)$ yields terminal MNN products with VEC = $18e^-$ so there is, *a priori*, no reason to expect one side of the reaction to be favored over the other.

As a variation on the theme of how the MO-based Lewis structures can be used to predict reaction energy trends, Figure 5 also considers the hydrogenation of $[1-M]_2(\mu-N_2)$ into two

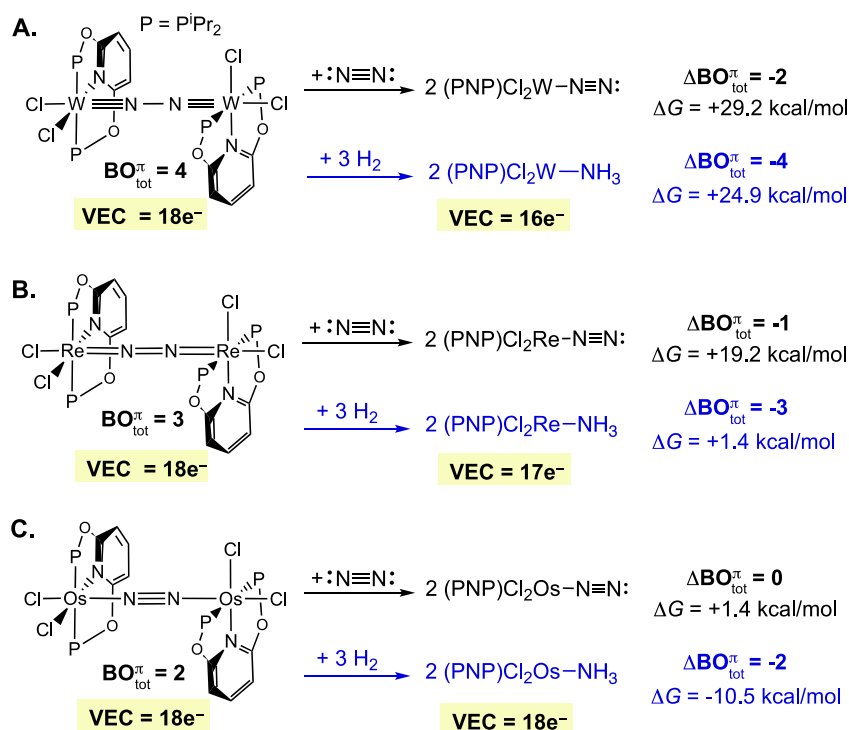


Figure 5. $\Delta \text{BO}_{\text{tot}}^{\pi}$ and energy trends in the reaction of $[1\text{-M}]_2(\mu\text{-N}_2)$ with N_2 and H_2 .

monomeric octahedral ammine complexes using three H_2 molecules. For the different metals, the same reaction is associated with a different change in the number of π -bonds: $\Delta \text{BO}_{\text{tot}}^{\pi} = -4$ (W), -3 (Re), and -2 (Os), so one would expect increasingly exergonic reactions across the series. This has been confirmed using new calculations, which afford: $\Delta G = +24.9$ (W), $+1.4$ (Re), and -10.5 (Os) kcal/mol.⁷² We see here that this transformation, hydrogenation of the bridging N_2 ligand, is counterintuitively *much more exergonic* for the complexes having N_2 bonds that are less “activated”.

LEWIS STRUCTURE AND THE SPLITTING OF $\mu\text{-N}_2$ COMPLEXES

The splitting of bridging N_2 into two nitriles is one of the most intriguing reactions in transition metal chemistry. The reaction was first discovered by Laplaza and Cummins in 1995 for $[5\text{-Mo}]_2(\mu\text{-N}_2)$ (Scheme 1B) upon treating the isolable three-coordinate fragment $\text{Mo}(\text{N}^i\text{BuAr})_3$ with N_2 .⁷³ The reaction is of immense interest because it suggests distinct pathways in catalytic N_2 reduction and functionalization.^{32,69,74–80} In this section we show how Lewis structures can greatly simplify the discussion of this reaction, and even bring new insights to understanding it. Instead of continuing our presentation with the octahedral complex $[1\text{-Re}]_2(\mu\text{-N}_2)$ which undergoes NN cleavage photolytically but not thermally, we chose to study Cummins’ original complex $[5\text{-Mo}]_2(\mu\text{-N}_2)$.

In order to discuss the splitting reaction, it is essential to have an orbital correlation diagram that tracks both the σ - and π -bonds in the reactants and products, which we present in Figure 6. Orbital correlation diagrams for this system were previously reported for $[5\text{-Mo}]_2(\mu\text{-N}_2)$,^{69,81,82} and have also proved useful in studies of metal-mediated oxygen atom transfer reactions.⁸³ Our own approach to the same type of diagram is detailed in this section. The $(3d_{xz}, 3d_{yz})$ AOs of each metal in $[5\text{-Mo}]_2(\mu\text{-N}_2)$ have the right symmetry and

orientation to undergo π -interactions with the $(2p_x, 2p_y)$ AOs of the bridging nitrogen, leading to the same qualitative π -MO diagram of the octahedral complexes in Figure 4. To construct the σ -MOs, we assume that the total σ -bonding in MNNM derives from one empty hybrid AO (ϕ) from each metal and the full $(2s, 2p_z)$ AOs from each nitrogen (total six AOs). To simplify the problem, we divide these into two subsets as shown on the left side of Figure 6. Subset 1 includes the two metal hybrid AOs and the two $2p_z$ AOs of nitrogen. Subset 2 includes the $2s$ AOs of nitrogen.

Subset 1 generates two bonding (σ_g and σ_u) and two antibonding (σ_g^* and σ_u^*) MOs delocalized over MNNM. Subset 2 generates two MOs localized on the nitrogen atoms and accordingly labeled as σ_{NN} and σ_{NN}^* . The MOs from the two sets that have the same symmetry are combined in brackets, $[\sigma_{\text{NN}}, \sigma_g]$ and $[\sigma_u^*, \sigma_{\text{NN}}^*]$, to indicate that these can mix, but that such mixing does not change the overall bonding/antibonding classification of the MOs. An important result from this analysis is that none of the unoccupied antibonding σ -type MOs have bonding character in M–N; σ_g^* and σ_u^* each have a node intersecting the M and N atoms. The σ - and π -MOs can now be combined. The number and character of the MOs is critical in developing a generic correlation diagram for MNNM splitting, but the precise energy level ordering is not consequential. We find it helpful to aggregate the π - and π^* -MOs above the σ and below the σ^* ones. Note that, for this specific complex, the $\delta\delta'$ -MOs derived from $(d_{xy}, d_{x^2-y^2})$ are omitted from the figure because these acquire high antibonding character due to mixing with the amido ligands.

The symmetry of the MOs in the correlation diagram can be preserved by aligning the MN bonds of the two nitrile products linearly as shown at the right of Figure 6. This makes it clear that MOs σ_g , σ_w , π_u , and π_g of MNNM, which are bonding in M–N, correlate with the two bonding σ_{MN} MOs

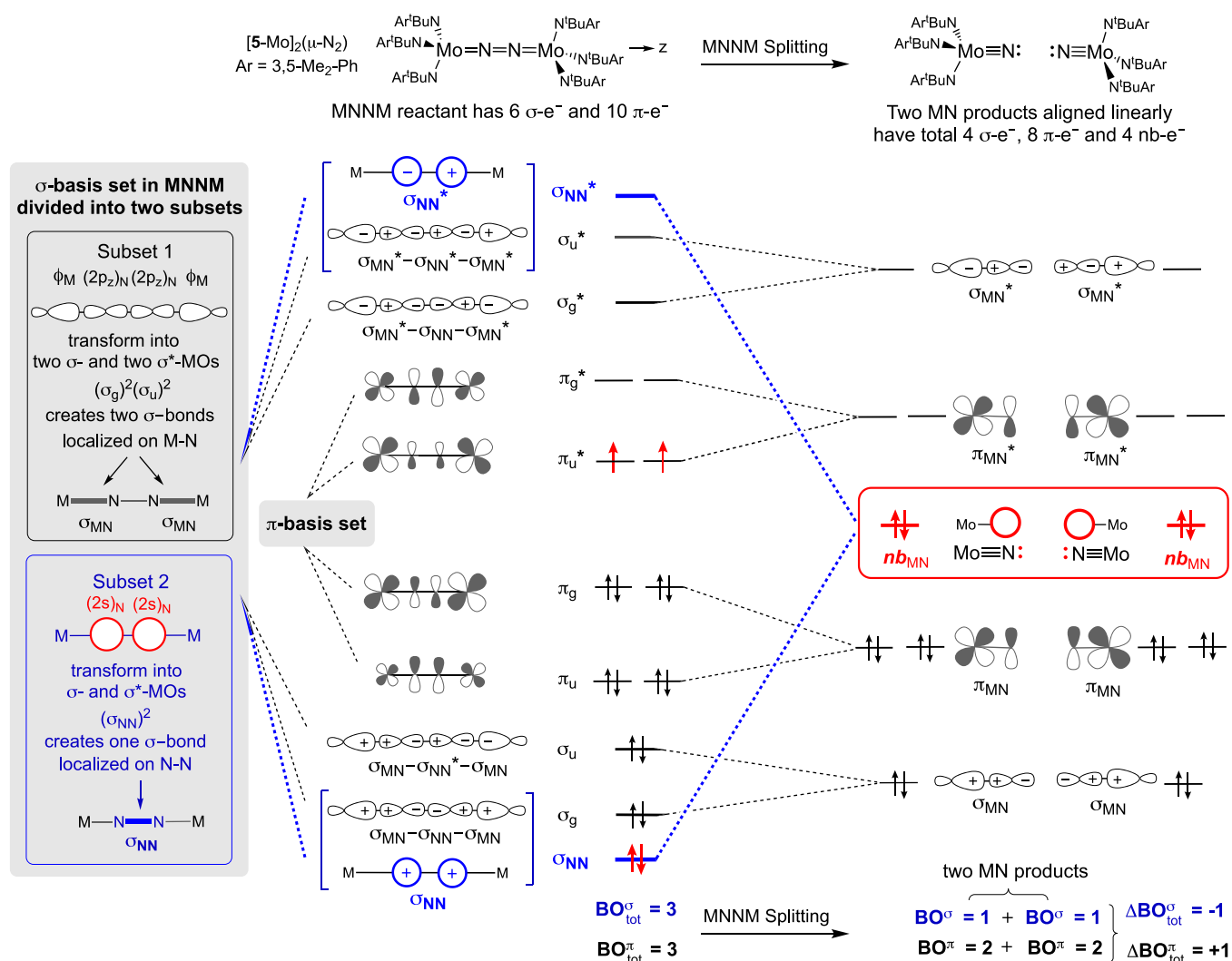


Figure 6. Orbital correlation diagram for splitting of $[\text{5-Mo}]_2(\mu\text{-N}_2)$ meant to clarify the nature of the σ - and π -MOs in the reactants and products; the aggregation of the π - and π^* -MOs above the σ and below the σ^* ones is arbitrary. The $\delta\delta'$ -MOs derived from $(d_{xy}, d_{x^2-y^2})$ have antibonding character in this system and are omitted. The π -MOs are doubly degenerate, but only one MO is drawn.

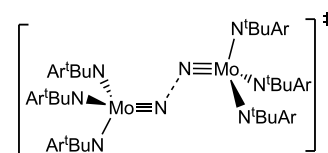
and the two bonding π_{MN} MOs of the products. On the other hand, MOs π_u^* , π_g^* , σ_g^* , and σ_u^* of MNNM, which are antibonding in M–N, correlate with the antibonding MOs σ_{MN}^* and π_{MN}^* of the nitrides. Lastly, and perhaps most importantly for our purposes, Figure 6 shows without ambiguity that MOs σ_{NN} and σ_{NN}^* of MNNM correlate with two nonbonding MOs in the MN products (nb_{MN}).

Figure 6 provides an opportunity to analyze how the bond order changes during N_2 splitting. $[\text{5-Mo}]_2(\mu\text{-N}_2)$ has 6 σ -electrons in $(\sigma_{NN})^2(\sigma_g)^2(\sigma_u)^2$ configuration leading to $\Delta\text{BO}_{\text{tot}}^{\sigma} = 3$. Population of σ_{NN} generates a bond localized between the two N atoms, and population of σ_g and σ_u generates two σ -bonds localized between the MN atoms (σ_{MN}). The π -system in this $\mu\text{-N}_2$ complex has 10 electrons in $(\pi_u)^4(\pi_g)^4(\pi_u^*)^2$ configuration leading to a ground state with $\text{BO}_{\text{tot}}^{\pi} = 3$ and two unpaired electrons, with one local π -bond in each MN and NN. The σ - and π -bonds add up to a $\text{Mo}=\text{N}=\text{N}=\text{Mo}$ Lewis structure. $[\text{5-Mo}]_2(\mu\text{-N}_2)$ is experimentally characterized to have a triplet spin ground state.²²

To achieve the splitting reaction of Figure 6, an electronic rearrangement within $[\text{5-Mo}]_2(\mu\text{-N}_2)$ can be envisioned that moves the two unpaired electrons from the doubly degenerate

π_u^* into σ_{NN}^* . Emptying π_u^* reduces the local NN BO^{π} to 0 and increases each local MN BO^{π} to 2. Filling σ_{NN}^* also drops BO^{σ} to 0; the resulting $(\sigma_{NN})^2(\sigma_{NN}^*)^2$ configuration indicates the electrons reside in effectively nonbonding orbitals that can be regarded as lone pairs (nb_{MN}). The combined effects lead to a $[\text{Mo}\equiv\text{N}::\text{N}\equiv\text{Mo}]$ Lewis structure—two separated metal nitride complexes.⁸⁴ The given reaction is symmetry and spin forbidden. Theoretical studies support a reaction pathway for splitting taking place via a trans bending mode of the MNNM core (zigzag transition state structure; Scheme 2) that relieves the orthogonality of the π - and σ -MOs from one plane of the linear structure.⁸⁵ In this specific system, rotation of the amido ligands was proposed to aid reaching the splitting transition state.⁸⁶

Scheme 2. Transition State Structure for MNNM Splitting



The general features of Figure 6, including the requirement of intersystem crossing, align with other reports on the mechanism of MNNM splitting.^{22,69,81,82} Our description does include a few subtle but important differences, however. Previous diagrams relied on using symmetry labels to correlate the MOs in the reactants, the bent transition state, and the products, but did not show the lone electron pairs of the nitride products. Instead, they matched a σ^* -MO in the μ -N₂ reactant with a bonding σ -MO in the nitride products suggesting the creation of one new MN σ -bond—but this cannot be correct! Figure 6 shows that MNNM splitting breaks one NN σ -bond. The discrepancy arises because the σ^* -MO in the commonly used correlation diagrams had been presented as having bonding character in MN and antibonding character in NN,²² often labeled as $\sigma_{\text{MN}}-\sigma_{\text{NN}}^*-\sigma_{\text{MN}}$.^{69,81,82} Figure 6 shows that the σ^* -MOs of MNNM cannot have MN σ -bonding character. The $\sigma_{\text{MN}}-\sigma_{\text{NN}}^*-\sigma_{\text{MN}}$ MO is the same filled bonding σ_u which contributes to making the M–N σ -bonds in MNNM; these bonds are retained in the products. The MO-based Lewis structures of [5-Mo]₂(μ -N₂) and the nitride product of cleavage also align with the bonding changes described in Figure 6. The N₂-bridged Lewis structure has three σ -bonds and three π -bonds across the MNNM core, while the two nitride complexes have one σ -bond and two π -bonds each, consistent with loss of a σ - σ bond and formation of one π -bond during splitting.

Ethylenedione provides a direct isolobal analogy with an organic system that is also linear as well as has a triplet ground state and an O=C=C=O Lewis structure (Figure 3). An elaborate CASSCF *ab initio* study by Gordon and co-workers taking into account spin-orbit coupling interactions showed this molecule to undergo splitting following intersystem crossing via a zigzag transition state having a geometry remarkably similar to the one reported for MNNM.⁶⁰ A quasi atomic orbital (QUAO) analysis provided a visual representation of how the CC MOs of the reactant evolve into two partially occupied carbon lone pairs in the transition state, and how two lone pairs eventually buildup at the carbons of the separated products, [O≡C: :C≡O].⁶⁰ This analysis is in full accord with the one presented in Figure 6 for MNNM splitting.

The MO view of the splitting reaction based on Figure 6 would be equally applicable to any end-on bridging N₂ complex with 10 π -electrons in an M=N=N=M Lewis structure. In fact, the important N₂ splitting reactivity has been reported only for complexes with $\text{BO}_{\text{tot}}^{\pi\sigma} = 3$, although the examples in Scheme 1A clearly indicate a 10 π -e[−] configuration alone is not sufficient for splitting. Using the MO-based Lewis structures to count the number of bonds and valence electrons provides a good starting point to discuss some of the observed reactivity patterns.

Figure 7 compares the change in the total σ - and π -bond orders ($\Delta\text{BO}_{\text{tot}}^{\pi\sigma}$) upon splitting of [5-Mo]₂(μ -N₂) and its dicationic congener, which is also known and crystallographically characterized.⁸⁶ The neutral complex has a Mo=N=N=Mo Lewis structure; when it splits into two neutral nitrides Mo≡N; the NN σ -bond is cleaved and a new π -bond is formed, amounting to $\Delta\text{BO}_{\text{tot}}^{\pi\sigma} = 0$. The bridging dication, on the other hand, has 8 π -e[−] in a $(\pi_u)^4(\pi_g)^4$ configuration yielding $\text{BO}_{\text{tot}}^{\pi} = 4$ and an [Mo≡N–N≡Mo]²⁺ Lewis structure. Despite the increasingly stretched NN bond and the double positive charge that one might anticipate to favor cleavage from a purely electrostatic perspective, this dication is

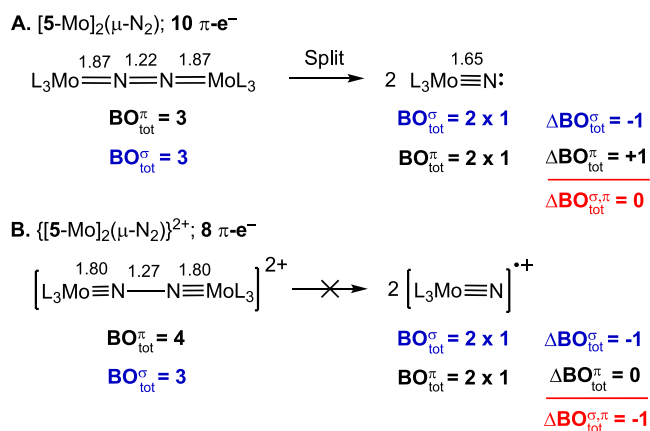


Figure 7. Change in the number of bonds upon splitting of [5-Mo]₂(μ -N₂) and its dication. Crystallographic bond lengths in Å.

stable at 20 °C both as a solid and in solution. NN splitting in this case breaks one σ -NN bond ($\Delta\text{BO}_{\text{tot}}^{\sigma} = -1$) without a change in the number of MN π -bonds ($\Delta\text{BO}_{\text{tot}}^{\pi} = 0$). Based on the net loss of a bond ($\Delta\text{BO}_{\text{tot}}^{\sigma,\pi} = -1$) one anticipates the reaction to be less exothermic than the splitting of the neutral [5-Mo]₂(μ -N₂).

In closing this section, we consider how factors beyond the bond order, such as the attributes of the bonds or effects from the ancillary ligands, can affect N₂ splitting reactivity. The fundamental principles that quantitatively govern the splitting of 10 π -electron M=N=N=M complexes are still being elucidated, but at least two additional factors beyond change in the number of bonds can influence the reaction. First, the 4d and 5d transition metals have strong capacity for MN π -bonding due to relativistic effects,⁸⁷ and thus the increase in the number of π -bonds upon splitting is particularly beneficial in terms of energetics. In the absence of such effects in 3d metals, loss of σ_{NN} is not well compensated for by the gain in π_{MN} . Accordingly, the vanadium complex [3-V]₂(μ -N₂) in Scheme 1A does not split even though it is structurally and electronically similar to [5-Mo]₂(μ -N₂).⁸⁸ Second, the splitting energies are highly dependent on the presence or absence of a ligand *trans* to the bridging N₂. For example, the 10 π -e[−] five-coordinate trigonal bipyramidal complex [4-Mo]₂(μ -N₂) in Scheme 1 has a 4d metal yet is not reported to undergo thermal splitting, in contrast to the facile cleavage of the closely related four-coordinate tetrahedral [5-Mo]₂(μ -N₂).⁸⁹ Likewise, thermal NN splitting has been observed for five-coordinate 10 π -e[−] complexes in square pyramidal geometries that leave a vacant coordination site *trans* to the N₂ bridge, as exemplified by Schneider's complex [6-Re]₂(μ -N₂) shown in Scheme 1B,^{90,91} but not for the octahedral complexes [1-Re]₂(μ -N₂) and [2-Re]₂(μ -N₂) in Scheme 1A.⁸¹ The nitride ligand has a very strong *trans* influence (induced by the exceptionally short MN bond length);⁹² thus N–N splitting is disfavored by the presence of a *trans* ligand.

■ ASSIGNING MO-DERIVED LEWIS STRUCTURES FOR OTHER GEOMETRIES

So far, we have focused on symmetrical octahedral and tetragonal μ -N₂ complexes. In our prior work, we assigned $\text{BO}_{\text{tot}}^{\pi\sigma}$ for 25 complexes ranging from three- to six-coordinate and covering 3d, 4d, and 5d transition metals.¹⁴ Representative examples are shown in Figure 8. The π -bonding picture was established using DFT methods coupled to experimental

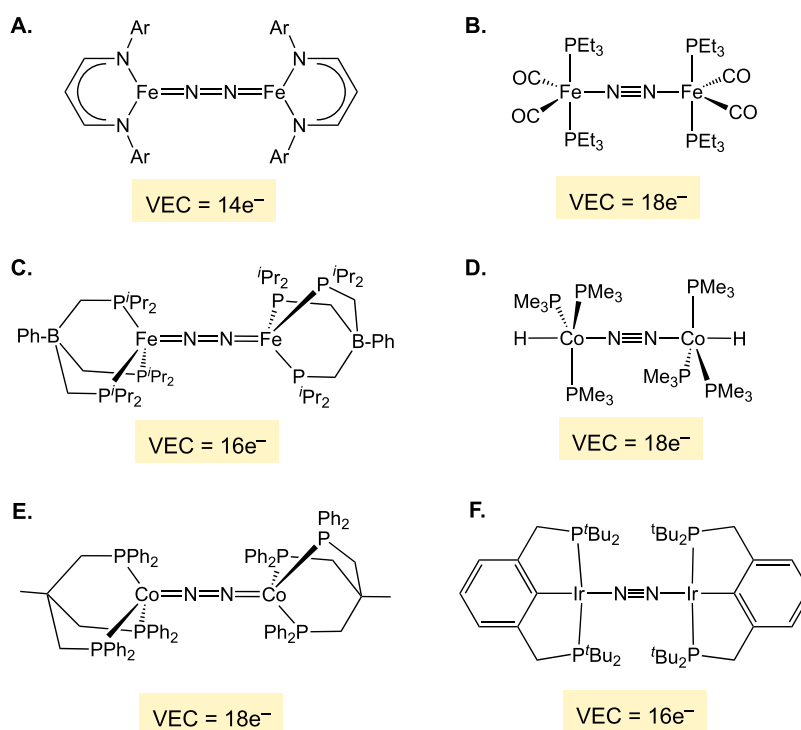


Figure 8. MO-based Lewis structures and VECs of selected $\mu\text{-N}_2$ complexes with different geometries.

spectroscopic data. Qualitative MO diagrams for some of the geometries are given in Figures SI-4–6 of this Perspective. In the following sections, we discuss some aspects of high-spin complexes, and we assign Lewis structures to two unique classes of complexes that we did not consider before, namely heterobimetallic complexes and metallocenes.

■ HIGH SPIN COMPLEXES

A prototype of a high-spin $\mu\text{-N}_2$ complex is the three-coordinate diiron(I) complex (Figure 8A) with a septet spin ground state.⁹³ This complex has a $10\pi\text{-e}^-$ configuration, so it is assigned an $\text{M}=\text{N}=\text{N}=\text{M}$ Lewis structure leading to a 14e^- VEC. The given Lewis assignment agrees with the experimentally observed substantial weakening of the NN bond that is much greater than in the lower-valent phosphine-carbonyl iron complex (Figure 8B).⁹⁴ For another example, we return to the octahedral complex $[\text{I-W}]_2(\mu\text{-N}_2)$. We discussed above (Figure 4) the singlet state of this complex from the $(\pi_u)^4(\pi_g)^4(\delta\delta')^4$ configuration where each metal provides 2e^- to the π -MOs and 2e^- to $\delta\delta'$. Alternatively, each metal may provide 3e^- to the π -manifold and only 1e^- to $\delta\delta'$ leading to a $(\pi_u)^4(\pi_g)^4(\delta\delta')^2(\pi_u^*)^2$ configuration. The additional partial occupancy of π_u^* lowers BO^π to 3, so the Lewis structure would be $\text{W}=\text{N}=\text{N}=\text{W}$. Consistently, the computed quintet state of $[\text{I-W}]_2(\mu\text{-N}_2)$ has longer WN (1.93 Å) and shorter NN (1.19 Å) bonds than the singlet state (1.83 and 1.24 Å respectively), such that the quintet state is very similar to the related $10\pi\text{-e}^-$ species $[\text{I-Re}]_2(\mu\text{-N}_2)$.¹⁴ Despite the lower $\Delta\text{BO}_{\text{tot}}^\pi$, the computed energy of the quintet spin state of $[\text{I-W}]_2(\mu\text{-N}_2)$ is only 8.5 kcal/mol higher than the closed shell singlet, suggesting similar energies associated with pairing two electrons in $\delta\delta'$ or promoting two electrons to π_u^* . Indeed, examples of $d^4\text{-d}^4\mu\text{-N}_2$ complexes with open-shell ground states are known,^{95,96} and a spin-state change had been proposed to initiate N_2 splitting.⁹⁵ The model can therefore be

valuable to predict differences in properties or reactivities as a function of spin state.

■ HETEROBIMETALLIC $\mu\text{-N}_2$ COMPLEXES

While qualitative π -MO diagrams can extract a $\text{BO}_{\text{tot}}^\pi$ term for known heterobimetallic $\mu\text{-N}_2$ complexes,^{97–102} some systems require Lewis structure representations distinct from the ones used for the symmetrical ones. For an illustrative example, we consider in Figure 9 the mixed Mo/Ti complex $[\text{S-MoTi}](\mu\text{-N}_2)$.

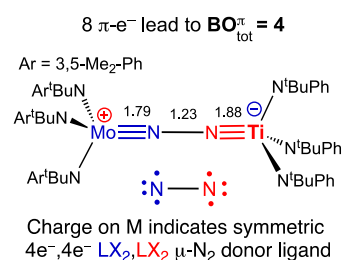


Figure 9. Lewis structure for the heterobimetallic complex $[\text{S-MoTi}](\mu\text{-N}_2)$. Crystallographic bond distances in Å.

N_2),¹⁰³ the direct analogue of the symmetrical $[\text{S-Mo}]_2(\mu\text{-N}_2)$ discussed above. The Mo/Ti complex is characterized by short MoN (1.79 Å) and TiN (1.88 Å) bonds, a significantly stretched NN bond (1.23 Å), and a quite low ν_{NN} (1575 cm^{-1}).¹⁰³

Starting with the same MO diagram of $[\text{S-Mo}]_2(\mu\text{-N}_2)$ derived in Figure 6 and then removing two electrons to account for titanium having two less electrons than Mo leads to a $(1\pi)^4(2\pi)^4$ configuration (the different metals prevents the use of π_u and π_g labels for the π -MOs in this case). The MoNTi core therefore has $\text{BO}_{\text{tot}}^\pi = 4$ with two π -bonds in each of MoN and TiN and none in NN, fully consistent with the experimental parameters. However, merely using the $\text{Mo}=\equiv$

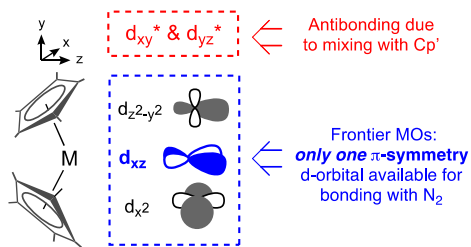
N–N≡Ti Lewis structure leads to unreasonable formal oxidation states, Mo^V and Ti^V, and unreasonable VECs.¹⁰⁴ A distinct Lewis structure representation is obviously needed to inform that the neutral Mo(N^tBuAr)₃ and Ti(N^tBuPh)₃ fragments provide different numbers of π electrons to the MoNNTi core, 3e⁻ and 1e⁻, respectively. We propose that this can be done by adding a positive and negative charge to the Mo and Ti centers. Within the ionic ligand formalism, the given Lewis representation implies an [N₂]⁴⁻ ligand and Mo^{VI}–Ti^{IV} oxidation states. Consistent with these assignments, the Mo–N bond distance of 1.79 Å [5-MoTi](μ -N₂) is essentially equal to that of the isoelectronic dicationic dimolybdenum [5-Mo]₂(μ -N₂)²⁺ (1.80 Å).

THE SPECIAL CASE OF METALLOCENES

Finally, we turn to the metallocenes of group 4 transition metals, which have a rich history in nitrogen fixation and exemplify some of the interesting features associated with geometric changes.^{105–108} We focus on the end-on bridging titanium complexes [Cp'₂Ti]₂(μ -N₂) (Cp' = substituted cyclopentadienyl). Depending on the substituents, these are known to have two limiting conformations in the solid state differentiated by whether the two Cp' rings on one metal are staggered (*D*_{2d}) or eclipsed (*D*_{2h}) with respect to the Cp' rings on the other metal.

In a bent metallocene fragment [Cp'₂M], the d_{xy}, d_{yz} AOs of the metal are used in bonding with the two η^5 -Cp' rings.¹⁰⁹ The remaining three metal d-AOs have their maximum probability density in the *xz* plane with largely d_{z²-y²}, d_{x²}, and d_{xz} character as depicted in Scheme 3.¹⁰⁹ There is therefore

Scheme 3. Frontier MOs in a Bent Metallocene^a



^aAdapted from ref 109.

only one d-orbital on each metal available for π -bonding in μ -N₂ metallocenes. This leads to MO diagrams that are dependent on the conformation as described in Figure 10.

The equivalent metals in the staggered [Cp'₂Ti]₂(μ -N₂) in Figure 10A are labeled Ti_A and Ti_B, and their Cp' ligands are positioned on the *x* and *y* axes, respectively. In this case, d_{yz} from Ti_A, d_{xz} from Ti_B, and the four (2p_x, 2p_y) AOs from N₂ generate three doubly degenerate π -MOs: one bonding (π), one nonbonding (π_{nb}), and one antibonding (π^*). The d_{x²} on Ti_A and d_{y²} on Ti_B combine into two nonbonding MOs that we label as $\sigma\sigma'$, like the $\delta\delta'$ labels used in Figure 4. Note that the d_{z²-y²} AO shown in Scheme 3 is used for σ -bonding with N₂; the resulting σ -MOs are not included in the final MO diagram. Because the opposing metal d-orbitals in Figure 10A are orthogonal to each other, there are two distinct π -systems that are degenerate, and the given picture of bridging π -bonding in Figure 10A is similar to the one in the terminal N₂ complexes in Figure 2 above: the degree of occupancy of the nonbonding π -MO does not influence BO_{tot} ^{π} and the Lewis structure. The

nonbonding character of both $\sigma\sigma'$ and π_{nb} as obtained from the simplified MO diagram suggests μ -N₂ metallocenes have accessible open shell ground state configurations and BO ^{π} = 2 implying Ti–N≡N–Ti Lewis structure and a VEC = 16e⁻. This result aligns with the spectroscopic and MO analysis of [Cp'^{*}₂Ti]₂(μ -N₂) reported by Bercau and co-workers, including the presence of unpaired electrons.¹¹⁰ If the valence π -MOs were bonding in character, as in the nonmetallocenes, they would have been greatly stabilized relative to $\sigma\sigma'$ leading to a closed shell ground state.

Drawing the staggered end-on N₂-bridged metallocenes as M–N≡N–M is in accord with the short N–N distances crystallographically determined for [Cp'^{*}₂Ti]₂(μ -N₂) (1.15 or 1.16 Å, depending on the unit cell). The formulation also accommodates the following reactivity observations: (i) Ti and Zr [Cp'₂M]₂(μ -N₂) complexes react with N₂ to form bridging [Cp'₂M(N₂)]₂(μ -N₂) as well as terminal Cp'₂M(N₂)₂ products, both of which are diamagnetic 18e⁻ species;¹¹¹ (ii) N₂ substitution is often facile in metallocenes, implicating relatively weak M–N bonds; and (iii) no examples of direct thermal or photolytic N₂ splitting to terminal nitride complexes have been reported. Interestingly, a different outcome is obtained for the eclipsed conformer, which is observed for several metallocenes such as [(C₅Me₄H)₂Ti]₂(μ -N₂).¹¹² The two metal d_{yz} AOs and the two 2p_y AOs of N₂ are now all coplanar, transforming into two bonding and two antibonding nondegenerate π -MOs (Figure 10B). An additional pair of π and π^* MOs is generated from the nitrogen 2p_x AOs which are orthogonal to the π -symmetry d-orbitals. According to this analysis, the eclipsed conformer has three π -bonds with a Ti=N=N=Ti Lewis structure. Note that, whereas staggered complexes [Cp'₂M(N₂)]₂(μ -N₂) are common, we are not aware of any complexes of this formula that adopt an eclipsed geometry, which would lead to a 19e⁻ VEC for each metal center. The modifications in the π -MO diagrams discussed in this section are also relevant when one metallocene is bridged by N₂ to a nonmetallocene.^{102,113}

CONCLUSIONS AND OUTLOOK

Bridging N₂ transition metal complexes have a vast and intricate chemistry, yet despite decades of intensive research, the principles that dictate their structure and reactivity are still being elucidated. Bonding in the linear MNNM core of these complexes leads to delocalized π -MOs with different numbers of nodes that define local MN and NN π -bond orders analogously to linear organic molecules. Such π -MO diagrams were used by Chatt and Richard in 1971,¹¹⁴ and in numerous subsequent studies to rationalize observed trends in the NN bond lengths and stretching vibrational frequencies.^{115–117} However, the generally accepted approach to assigning Lewis structures for the MNNM cores has been based on empirical comparisons of the bond length or vibrational frequency of the bridging N₂ with those of free diazene or hydrazine. We note that the N–N bonds in linear MNNM cores are not comparable to the N–N single bond in hydrazine or the N=N double bond in diazene, just as the C–C bonds in diacetylene or ethylenedione are not comparable to those of ethane or ethylene. Instead of relying on this imperfect comparison to assign Lewis structures, we introduce an alternative model to assign Lewis structures based on qualitative π -MO diagrams. The model affords three limiting Lewis structures depending on the occupancy of the MOs: M–N≡N–M, M=N=N=M, and M≡N–N≡M.

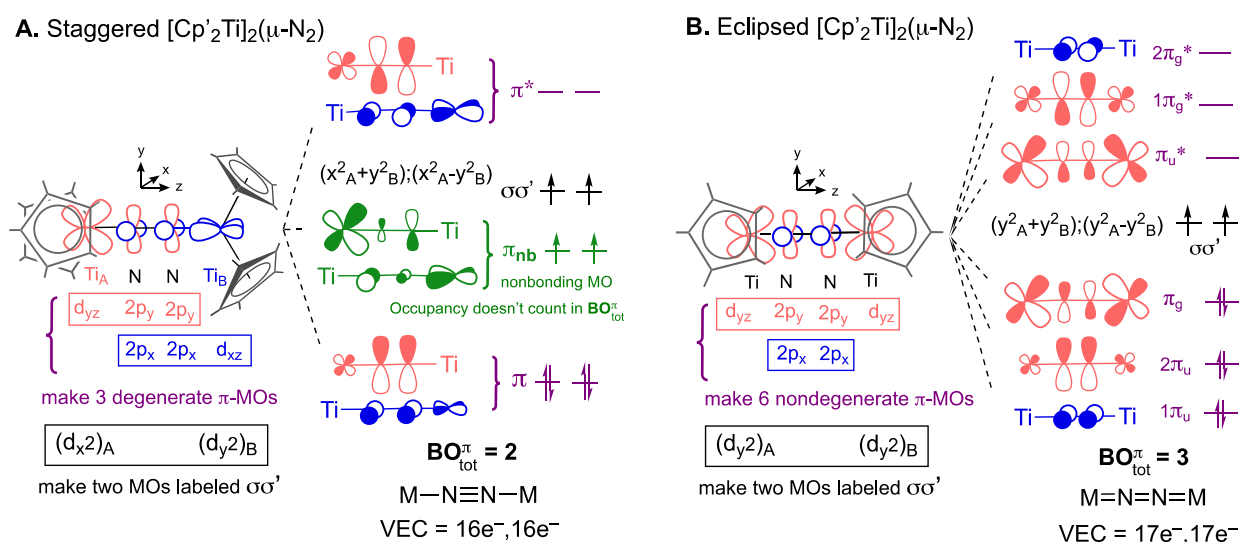


Figure 10. π -MO diagrams for staggered and eclipsed $[\text{Cp}'_2\text{Ti}]_2(\mu\text{-N}_2)$.

The MO-based Lewis structures lead to a new classification of $\mu\text{-N}_2$ complexes that we hope will enable meaningful comparisons across the field for the first time. With this new classification system, for example, we can now assign reliable electron donor numbers to the $\mu\text{-N}_2$ ligand and engage in familiar valence electron- and bond-counting exercises to aid understanding and predict reactivity trends of $\mu\text{-N}_2$ complexes. This was illustrated for several important reactions of bridging N_2 complexes: reaction with N_2 to give two terminal MN_2 products; reaction with H_2 to give the corresponding NH_3 adducts; and the splitting of MNNM into two metal nitrides. The MO-based model is broadly applicable across the periodic table and accommodates a wide variety of structural variations (e.g., coordination number, metallocenes, and heterobimetallic complexes). Computational DFT and *ab initio* methods will always be needed for quantitative purposes.¹¹⁸ However, the simple tools of tracking the number of bonds and VECs which are possible only with reliable Lewis structures can help advance the field by providing an intuitive understanding of bonding and reactivity patterns and providing a tool for “back of the envelope” predictions that can help rationalize reaction outcomes and guide the design of new catalysts.

■ ASSOCIATED CONTENT

Supporting Information

The Supporting Information is available free of charge at <https://pubs.acs.org/doi/10.1021/jacs.2c12243>.

Figures for MO displays and qualitative MO diagrams. Cartesian coordinates and absolute energies of the new molecules used to calculate the hydrogenation energies in Figure 5 (PDF)

■ AUTHOR INFORMATION

Corresponding Authors

Faraj Hasanayn – Department of Chemistry, American University of Beirut, Beirut 1107 2020, Lebanon; orcid.org/0000-0003-3308-7854; Email: fh19@aub.edu.lb

Alexander J. M. Miller – Department of Chemistry, University of North Carolina at Chapel Hill, Chapel Hill, North

Carolina 27599-3290, United States; orcid.org/0000-0001-9390-3951; Email: ajmm@email.unc.edu

Authors

Patrick L. Holland – Department of Chemistry, Yale University, New Haven, Connecticut 06520, United States; orcid.org/0000-0002-2883-2031

Alan S. Goldman – Department of Chemistry and Chemical Biology, Rutgers, The State University of New Jersey, New Brunswick, New Jersey 08903, United States; orcid.org/0000-0002-2774-710X

Complete contact information is available at: <https://pubs.acs.org/10.1021/jacs.2c12243>

Notes

The authors declare no competing financial interest.

■ ACKNOWLEDGMENTS

This work was supported through the NSF Chemical Catalysis program under Grant Nos. CHE-1954254, CHE-1954942, and CHE-1955014. Additional support was provided by the *Alwaleed Center for American Studies and Research* at AUB. We thank Robert H. Crabtree and John J. Curley for helpful discussions.

■ REFERENCES

- (1) Fritz Haber – Nobel Lecture. NobelPrize.org <https://www.nobelprize.org/prizes/chemistry/1918/haber/lecture/> (accessed Jan, 2023).
- (2) Grand View Research Ammonia Market Size, Share & Trends Analysis Report By Product Form (Liquid, Gas, Powder), By Application (Fertilizers, Textile, Pharmaceuticals, Refrigerants), By Region, And Segment Forecasts 2018–2025; Report ID: GVR-2-68038-207-5. <https://www.grandviewresearch.com/industry-analysis/ammonia-market> (accessed Jan, 2023).
- (3) Hochman, G.; Goldman, A. S.; Felder, F. A.; Mayer, J. M.; Miller, A. J. M.; Holland, P. L.; Goldman, L. A.; Manocha, P.; Song, Z.; Aleti, S. Potential Economic Feasibility of Direct Electrochemical Nitrogen Reduction as a Route to Ammonia. *ACS Sustain. Chem. Eng.* **2020**, *8*, 8938–8948.
- (4) Valera-Medina, A.; Amer-Hatem, F.; Azad, A. K.; Dedoussi, I. C.; de Joannon, M.; Fernandes, R. X.; Glarborg, P.; Hashemi, H.; He, X.; Mashruk, S.; McGowan, J.; Mounaim-Rousellet, C.; Ortiz-Prado, A.;

- Ortiz-Valera, A.; Rossetti, I.; Shu, B.; Yehia, M.; Xiao, H.; Costa, M. Review on Ammonia as a Potential Fuel: From Synthesis to Economics. *Energy Fuels* **2021**, *35*, 6964–7029.
- (5) Dunn, P. L.; Cook, B. J.; Johnson, S. L.; Appel, A. M.; Bullock, M. R. Oxidation of Ammonia with Molecular Complexes. *J. Am. Chem. Soc.* **2020**, *142*, 17845–17858.
- (6) Jewess, M.; Crabtree, R. H. Electrocatalytic Nitrogen Fixation for Distributed Fertilizer Production? *ACS Sustain. Chem. Eng.* **2016**, *4*, 5855–5858.
- (7) Maserio, F.; Perrin, M. A.; Dey, S.; Mougel, V. Dinitrogen Fixation: Rationalizing Strategies Utilizing Molecular Complexes. *Chem.—Eur. J.* **2021**, *27*, 3892–3928.
- (8) Hidai, M.; Mizobe, Y. Recent Advances in the Chemistry of Dinitrogen Complexes. *Chem. Rev.* **1995**, *95*, 1115–1133.
- (9) Yang, J.-H.; Peng, M.; Zhai, D.-D.; Xiao, D.; Shi, Z.-J.; Yao, S.; Ma, D. Fixation of N₂ into Value-Added Organic Chemicals. *ACS Catal.* **2022**, *12*, 2898–2906.
- (10) Kim, S.; Loose, F.; Chirik, P. J. Beyond Ammonia: Nitrogen–Element Bond Forming Reactions with Coordinated Dinitrogen. *Chem. Rev.* **2020**, *120*, 5637–5681.
- (11) Chalkley, M. J.; Drover, M. W.; Peters, J. C. Catalytic N₂-to-NH₃ (or -N₂H₄) Conversion by Well-Defined Molecular Coordination Complexes. *Chem. Rev.* **2020**, *120*, 5582–5636.
- (12) Mézailles, M. Reactivity and Structure of Complexes of Small Molecules: Dinitrogen. *Comprehensive Coordination Chemistry III*, 3rd ed.; 2021; pp 875–958. DOI: 10.1016/B978-0-08-102688-5.00083-0.
- (13) Burford, R. J.; Fryzuk, M. D. Examining the Relationship between Coordination Mode and Reactivity of Dinitrogen. *Nat. Rev. Chem.* **2017**, *1*, 0026.
- (14) Yamout, S. L.; Ataya, M.; Hasanayn, F.; Holland, P. L.; Miller, A. J. M.; Goldman, A. S. Understanding Terminal versus Bridging End-on N₂ Coordination in Transition Metal Complexes. *J. Am. Chem. Soc.* **2021**, *143*, 9744–9757.
- (15) Fryzuk, M. D. Side-on End-on Bound Dinitrogen: An Activated Bonding Mode That Facilitates Functionalizing Molecular Nitrogen. *Acc. Chem. Res.* **2009**, *42*, 127–133.
- (16) Fryzuk, M. D.; Haddad, T. S.; Mylvaganam, M.; McConville, D. H.; Rettig, S. J. End-on versus Side-on Bonding of Dinitrogen to Dinuclear Early Transition-Metal Complexes. *J. Am. Chem. Soc.* **1993**, *115*, 2782–2792.
- (17) Evans, W. J.; Ulibarri, T. A.; Ziller, W. J. Isolation and x-ray crystal structure of the first dinitrogen complex of an f-element metal, [(C₅Me₅)₂Sm]₂N₂. *J. Am. Chem. Soc.* **1988**, *110*, 6877–6879.
- (18) MacLachlan, E. A.; Fryzuk, M. D. Synthesis and Reactivity of Side-On-Bound Dinitrogen Metal Complexes. *Organometallics* **2006**, *25*, 1530–1543.
- (19) Blomberg, M. R. A.; Siegbahn, P. E. M. Bridge Bonding of N₂ to Dinuclear Transition Metal Systems. *J. Am. Chem. Soc.* **1993**, *115*, 6908–6915.
- (20) Treitel, I. M.; Flood, M. T.; Marsh, R. E.; Gray, H. B. Molecular and Electronic Structure of μ -Nitrogen-Decaamminediruthenium(II). *J. Am. Chem. Soc.* **1969**, *91*, 6512–6513.
- (21) Powell, C. B.; Hall, M. B. Molecular Orbital Calculations on Dinitrogen-Bridged Transition-Metal Dimers. *Inorg. Chem.* **1984**, *23*, 4619–4627.
- (22) Laplaza, C. E.; Johnson, M. J. A.; Peters, J. C.; Odom, A. L.; Kim, E.; Cummins, C. C.; George, G. N.; Pickering, I. J. Dinitrogen Cleavage by Three-Coordinate Molybdenum(III) Complexes: Mechanistic and Structural Data. *J. Am. Chem. Soc.* **1996**, *118*, 8623–8638.
- (23) Frenking, G.; Fröhlich, N. The nature of the bonding in transition-metal compounds. *Chem. Rev.* **2000**, *100*, 717–774.
- (24) Dewar, M. J. S. A Review of the π -complex Theory. *Bull. Soc. Chim. Fr.* **1951**, *18*, C79.
- (25) Chatt, J.; Duncanson, L. A. Olefin coordination compounds. Part III. Infrared spectra and structure: attempted preparation of acetylene complexes. *J. Chem. Soc.* **1953**, 2939–2947.
- (26) Chatt, J.; Dilworth, J. R.; Richards, R. Recent Advances in the Chemistry of Nitrogen Fixation. *Chem. Rev.* **1978**, *78*, 589–626.
- (27) Holland, P. L. Metal-dioxygen and metal-dinitrogen complexes: where are the electrons? *Dalton Transactions* **2010**, *39*, 5415–5425.
- (28) Weber, J. E.; Bhutto, S. M.; Genoux, A. T.-Y.; Holland, P. L. Dinitrogen Binding and Functionalization. In *Comprehensive Organometallic Chemistry IV*; Vol. 1; Elsevier, 2022; pp 521–554. DOI: 10.1016/b978-0-12-820206-7.00068-8.
- (29) Tatsumi, T.; Hidai, M.; Uchida, Y. Preparation and properties of dinitrogen-molybdenum complexes. II. Dinitrogen(organonitrile) complexes of molybdenum. *Inorg. Chem.* **1975**, *14*, 2530–2534.
- (30) Klopsch, I.; Yuzik-Klimova, E. Y.; Schneider, S. Functionalization of N₂ by Mid to Late Transition Metals via N–N Bond Cleavage. *Topics in Organometallic Chemistry*; Elsevier: 2017; Vol. 60, p 71. DOI: 10.1007/3418_2016_12.
- (31) Singh, D.; Buratto, W. R.; Torres, J. F.; Murray, L. J. Activation of Dinitrogen by Polynuclear Metal Complexes. *Chem. Rev.* **2020**, *120*, 5517–5581.
- (32) Forrest, S. J. K.; Schluschaß, B.; Yuzik-Klimova, E. Y.; Schneider, S. Nitrogen Fixation via Splitting into Nitrido Complexes. *Chem. Rev.* **2021**, *121*, 6522–6587.
- (33) Lewis, G. N. *Valence and The Structure of Atoms and Molecules*; The Chemical Catalog Company: 1923. ISBN-10:0598985409, ISBN-13:9780598985408.
- (34) Fischer, E. O.; Jira, R. How metallocene chemistry and research began in Munich. *J. Organomet. Chem.* **2001**, *637*, 7–12.
- (35) Werner, H. At Least 60 Years of Ferrocene: The Discovery and Rediscovery of the Sandwich Complexes. *Angew. Chem., Int. Ed.* **2012**, *51*, 6052–6058.
- (36) Hoffmann, R. Building Bridges Between Inorganic and Organic Chemistry. *Angew. Chem., Int. Ed.* **1982**, *21*, 711–724.
- (37) Bruch, Q. J.; Connor, G. P.; Chen, C.-H.; Holland, P. L.; Mayer, J. M.; Hasanayn, F.; Miller, A. J. M. Dinitrogen Reduction to Ammonium at Rhenium Utilizing Light and Proton-Coupled Electron Transfer. *J. Am. Chem. Soc.* **2019**, *141*, 20198–20208.
- (38) Streitwieser, A. *Molecular Orbital Theory for Organic Chemists*; John Wiley & Sons, 1961.
- (39) Albright, T. A.; Burdett, J. K.; Whangbo, M.-H. *Orbital Interactions in Chemistry*, 2nd ed.; John Wiley & Sons, 2013. DOI: 10.1002/9781118558409.
- (40) Mayer, I. Bond Order and Valence Indices: A Personal Account. *J. Comput. Chem.* **2007**, *28*, 204–221.
- (41) McQuarrie, D. A.; Simon, J. D. *Physical Chemistry A Molecular Approach*, 1st ed.; University Science Books. Ca., 1997.
- (42) Allen, A. D.; Senoff, C. W. Nitrogenopentammineruthenium-(II) Complexes. *Chem. Commun.* **1965**, 621–622.
- (43) Bottomley, F.; Nyburg, S. C. Molecular Nitrogen as a Ligand: the Crystal Structure of Nitrogenpentammineruthenium(II) Dichloride. *Chem. Commun.* **1966**, 897–898.
- (44) Fergusson, J. E.; Love, J. L.; Robinson, W. T. The Crystal and Molecular Structure of Dinitrogenpentaammineosmium(II) Chloride, [Os(NH₃)₅N₂]Cl₂, and Related Ruthenium Complexes. *Inorg. Chem.* **1972**, *11*, 1662–1666.
- (45) Libit, L.; Hoffmann, R. Detailed orbital theory of substituent effects. Charge transfer, polarization, and the methyl group. *J. Am. Chem. Soc.* **1974**, *96*, 1370–1383.
- (46) DuBois, D. L.; Hoffmann, R. Diazenido, Dinitrogen and Related Complexes. *Nouv. J. Chim.* **1977**, *1*, 479–492.
- (47) Chen, Z. Graphical Representation of Hückel Molecular Orbitals. *J. Chem. Educ.* **2020**, *97*, 448–456.
- (48) Tay, R.; Metha, G. F.; Shanks, F.; McNaughton, D. Determination of the Molecular Structure of Diacetylene from High-Resolution FTIR Spectroscopy. *Struct. Chem.* **1995**, *6*, 47–55.
- (49) Thorwirth, S.; Harding, M. E.; Muders, D.; Gauss, J. The empirical equilibrium structure of diacetylene. *J. Mol. Spectrosc.* **2008**, *251*, 220–223.
- (50) Coulson, C. A.; Jacobs, J. Electronic levels in simple conjugated systems II. Butadiene. *Proc. Royal. Soc.* **1951**, *206*, 146–153.
- (51) Kuchitsu, K., Ed. *Structure of Free Polyatomic Molecules - Basic Data*; Springer: Berlin, 1998. DOI: 10.1007/978-3-642-45748-7.

- (52) Anslyn, E. V.; Dougherty, D. A. *Modern Physical Organic Chemistry*; University Science Books: Sausalito, CA, 2006.
- (53) Robert, J. D.; Caserio, M. C. *Basic Principles of Organic Chemistry*, 2nd ed.; W. A. Benjamin, Inc.: Menlo Park, CA, 1977. [https://chem.libretexts.org/Bookshelves/Organic_Chemistry/Book%3A_Basic_Principles_of_Organic_Chemistry_\(Roberts_and_Caserio\)](https://chem.libretexts.org/Bookshelves/Organic_Chemistry/Book%3A_Basic_Principles_of_Organic_Chemistry_(Roberts_and_Caserio)).
- (54) Pople, J. A.; Santry, D. P. A molecular orbital theory of hydrocarbons II. Ethane, ethylene and acetylene. *Mol. Phys.* **1965**, *8*, 1362–3028.
- (55) Vermeeren, P.; van Zeist, W.-J.; Hamlin, T. A.; Fonseca Guerra, C.; Bickelhaupt, F. M. Not Carbon s–p Hybridization, but Coordination Number Determines C–H and C–C Bond Length. *Chem. - Eur. J.* **2021**, *27*, 7074–7079.
- (56) Craig, N. C.; Groner, P.; McKean, D. C. Equilibrium Structures for Butadiene and Ethylene: Compelling Evidence for π -Electron Delocalization in Butadiene. *J. Phys. Chem. A* **2006**, *110*, 7461–7469.
- (57) Cardozo, T. M.; Freitas, G. N.; Nascimento, M. A. C. Interference effect and the nature of the pi-bonding in 1,3-butadiene. *J. Phys. Chem. A* **2010**, *114*, 8798–8805.
- (58) Gu, J.; Wu, W.; Danovich, D.; Hoffmann, R.; Tsuji, Y.; Shaik, S. Valence bond theory reveals hidden delocalized diradical character of polyenes. *J. Am. Chem. Soc.* **2017**, *139*, 9302–9316.
- (59) Torrie, B. H.; Powell, B. M. Cyanogen: structure, dynamics and inter-molecular potentials. *J. Phys.: Condens. Matter* **1989**, *1*, 5827–5835.
- (60) Mato, J.; Poole, D.; Gordon, M. S. Stability and Dissociation of Ethylenedione (OCCO). *J. Phys. Chem. A* **2020**, *124*, 8209–8222.
- (61) Bürger, H.; Senzlober, M.; Sommer, S. Ground state and equilibrium structure of FCCF from high-resolution IR spectra of F¹²C¹³CF. *J. Mol. Spectrosc.* **1994**, *164*, 570–573.
- (62) Schluschaß, B.; Bortner, J.-H.; Rupp, S.; Demeshko, S.; Herwig, C.; Limberg, C.; Maciulis, N. A.; Schneider, J.; Würtele, C.; Krewald, V.; Schwarzer, D.; Schneider, S. Cyanate Formation via Photolytic Splitting of Dinitrogen. *JACS Au* **2021**, *1*, 879–894.
- (63) Kilgore, U. J.; Yang, X.; Tomaszewski, J.; Huffman, J. C.; Mindiola, D. J. Activation of Atmospheric Nitrogen and Azobenzene N=N Bond Cleavage by a Transient Nb(III) Complex. *Inorg. Chem.* **2006**, *45*, 10712–10721.
- (64) Green, M. L. H. A New Approach to the Formal Classification of Covalent Compounds of the Elements. *J. Organomet. Chem.* **1995**, *500*, 127–148.
- (65) Green, M. L. H.; Parkin, G. Application of the Covalent Bond Classification Method for the Teaching of Inorganic Chemistry. *J. Chem. Educ.* **2014**, *91*, 807–816.
- (66) Parkin, G. Classification of Organotransition Metal Compounds. In *Comprehensive Organometallic Chemistry III*; Crabtree, R. H., Mingos, D. M. P., Eds.; Elsevier: Oxford, 2007; Vol. 1, Chapter 1. DOI: 10.1016/B0-08-045047-4/00001-7.
- (67) Schröder, D.; Heinemann, C.; Schwarz, H.; Harvey, J. N.; Dua, S.; Blanksby, S. J.; Bowie, J. H. Ethylenedione: An Intrinsically Short-Lived Molecule. *Chem. - Eur. J.* **1998**, *4*, 2550–2557.
- (68) Wentrup, C.; Kambouris, P.; Evans, R. A.; Owen, D.; Macfarlane, G.; Chucho, J.; Pommelet, J. C.; Cheikh, A. B.; Plisnier, M.; Flammang, R. 2,5-Dithiacyclopentylideneketene and Ethenedithione, S=C=C=S, Generated by Flash Vacuum Pyrolysis. *J. Am. Chem. Soc.* **1991**, *113*, 3130–3135.
- (69) Bruch, Q. J.; Connor, G. P.; McMillion, N. D.; Goldman, A. S.; Hasanayn, F.; Holland, P. L.; Miller, A. J. M. Considering Electrocatalytic Ammonia Synthesis via Bimetallic Dinitrogen Cleavage. *ACS Catal.* **2020**, *10*, 10826–10846.
- (70) Liptrot, D. J.; Power, P. P. London dispersion forces in sterically crowded inorganic and organometallic molecules. *Nat. Rev. Chem.* **2017**, *1*, 0004.
- (71) Mears, K. L.; Power, P. P. Beyond Steric Crowding: Dispersion Energy Donor Effects in Large Hydrocarbon Ligands. *Acc. Chem. Res.* **2022**, *55*, 1337–1348.
- (72) The hydrogenation results were obtained using the same density functional (M06L) and basis set (def2-TZVP) previously used with the other N₂ coordination reaction.
- (73) Laplaza, C. E.; Cummins, C. C. Dinitrogen Cleavage by a Three-Coordinate Molybdenum(III) Complex. *Science* **1995**, *268*, 861–863.
- (74) Katayama, A.; Ohta, T.; Wasada-Tsutsui, Y.; Inomata, T.; Ozawa, T.; Ogura, T.; Masuda, H. Dinitrogen-Molybdenum Complex Induces Dinitrogen Cleavage by One-Electron Oxidation. *Angew. Chem., Int. Ed.* **2019**, *58*, 11279–11284.
- (75) Arashiba, K.; Eizawa, A.; Tanaka, H.; Nakajima, K.; Yoshizawa, K.; Nishibayashi, Y. Catalytic Nitrogen Fixation via Direct Cleavage of Nitrogen-Nitrogen Triple Bond of Molecular Dinitrogen under Ambient Reaction Conditions. *Bull. Chem. Soc. Jpn.* **2017**, *90*, 1111–1118.
- (76) Wagner, H. K.; Wadepohl, H.; Ballmann, J. Molybdenum-Mediated N₂-Splitting and Functionalization in the Presence of a Coordinated Alkyne. *Angew. Chem., Int. Ed.* **2021**, *60*, 25804–25808.
- (77) Bennaamane, S.; Espada, M. F.; Mulas, A.; Personeni, T.; Saffon-Merceron, N.; Fustier-Boutignon, M.; Bucher, C.; Mezailles, N. Catalytic Reduction of N₂ to Borylamine at a Molybdenum Complex. *Angew. Chem., Int. Ed. Engl.* **2021**, *60*, 20210–20214.
- (78) Zhang, G.; Liu, T.; Song, J.; Quan, Y.; Jin, L.; Si, M.; Liao, Q. N₂ Cleavage on d⁴/d⁴ Molybdenum Centers and Its Further Conversion into Iminophosphorane under Mild Conditions. *J. Am. Chem. Soc.* **2022**, *144*, 2444–2449.
- (79) Rebreyend, C.; de Bruin, B. Photolytic N₂ Splitting: A Road to Sustainable NH₃ Production? *Angew. Chem., Int. Ed.* **2015**, *54*, 42–44.
- (80) Bruch, Q. J.; Malakar, S.; Goldman, A. S.; Miller, A. J. M. Mechanisms of Electrochemical N₂ Splitting by a Molybdenum Pincer Complex. *Inorg. Chem.* **2022**, *61*, 2307–2318.
- (81) Schendzielorz, F.; Finger, M.; Abbenseth, J.; Würtele, C.; Krewald, V.; Schneider, S. Metal-Ligand Cooperative Synthesis of Benzonitrile by Electrochemical Reduction and Photolytic Splitting of Dinitrogen. *Angew. Chem., Int. Ed.* **2019**, *58*, 830–834.
- (82) Krewald, V. Dinitrogen photoactivation: status quo and future perspectives. *Dalton Trans.* **2018**, *47*, 10320–10329.
- (83) Veige, A. S.; Slaughter, L. G. M.; Lobkovsky, E. B.; Wolczanski, P. T.; Matsunaga, N.; Decker, S. A.; Cundari, T. R. Symmetry and Geometry Considerations of Atom Transfer: Deoxygenation of (Silox)₃WNO and R₃PO (R = Me, Ph, tBu) by (Silox)₃M (M = V, NbL (L = PMe₃, 4-Picoline), Ta; Silox = tBu₃SiO). *Inorg. Chem.* **2003**, *42*, 6204–6224.
- (84) Amido RR'N ligands can act either as X-type ligands (M–NRR'; one electron donor) or as LX-type ligands (M=NRR'; three electron donor) depending on the availability of empty valence AOs on the metal with matching symmetry. Crystallographic data reveal planar amido moieties in [5-Mo]₂(μ -N₂) and the splitting nitride product [(NRR')MoN] and that the amido planes are oriented in a propeller mode imparting local C₃ symmetry around each metal center. In this symmetry, the three filled amido π -donor AOs transform into one nondegenerate and one doubly degenerate ligand group orbitals (LGOs) of *a* and *e* symmetry, respectively. These LGOs have the correct symmetry to mix with the metal d_{z²} and (d_{xy}, d_{x²-y²}) AOs (the latter are treated as empty δ -MOs in Figure 6). The valence MOs of [5-Mo]₂(μ -N₂) in Figure 9 in ref 86 supports a small degree of mixing between the *a*-LGO and the d_{z²} AO. The three amido ligands on a given metal can therefore be thought to donate 9 electrons to the metal in the given systems. Using this counting scheme for the three amido ligands affords a VEC = 18 e⁻ on each metal in the bridging complex [5-Mo]₂(μ -N₂) and in the splitting product [(NRR')MoN].
- (85) Cui, Q.; Musaev, D. G.; Svensson, M.; Sieber, S.; Morokuma, K. N₂ Cleavage by Three-Coordinate Group 6 Complexes. W(III) Complexes Would Be Better Than Mo(III) Complexes. *J. Am. Chem. Soc.* **1995**, *117*, 12366–12367.
- (86) Curley, J. J.; Cook, T. R.; Reece, S. Y.; Müller, P.; Cummins, C. C. Shining Light on Dinitrogen Cleavage: Structural Features, Redox

Chemistry, and Photochemistry of the Key Intermediate Bridging Dinitrogen Complex. *J. Am. Chem. Soc.* **2008**, *130*, 9394–9405.

(87) Neyman, K. M.; Nasluzov, V. A.; Hahn, J.; Landis, C. R.; Rösch, N. Density Functional Study of N₂ Activation by Molybdenum(III) Complexes. Unusually Strong Relativistic Effects in 4d Metal Compounds. *Organometallics* **1997**, *16*, 995–1000.

(88) Tran, B. L.; Pinter, B.; Nichols, A. J.; Konopka, F. T.; Thompson, R.; Chen, C. H.; Krzystek, J.; Ozarowski, A.; Telsner, J.; Baik, M. H.; Meyer, K.; Mindiola, D. J. A Planar Three-Coordinate Vanadium(II) Complex and the Study of Terminal Vanadium Nitrides from N₂: A Kinetic or Thermodynamic Impediment to NN Bond Cleavage? *J. Am. Chem. Soc.* **2012**, *134*, 13035–13045.

(89) Shih, K.-Y.; Schrock, R. R.; Kempe, R. Synthesis of Molybdenum Complexes That Contain Silylated Triamidoamine Ligands. A μ -Dinitrogen Complex, Methyl and Acetylide Complexes, and Coupling of Acetylides. *J. Am. Chem. Soc.* **1994**, *116*, 8804–8805.

(90) Klopsch, I.; Finger, M.; Würtele, C.; Milde, B.; Werz, D. B.; Schneider, S. Dinitrogen Splitting and Functionalization in the Coordination Sphere of Rhenium. *J. Am. Chem. Soc.* **2014**, *136*, 6881–6883.

(91) Lindley, B. M.; van Alten, R. S.; Finger, M.; Schendzielorz, F.; Würtele, C.; Miller, A. J. M.; Siewert, I.; Schneider, S. Mechanism of Chemical and Electrochemical N₂ Splitting by a Rhenium Pincer Complex. *J. Am. Chem. Soc.* **2018**, *140*, 7922–7935.

(92) Coe, B. J.; Glenwright, S. J. Trans-Effects in Octahedral Transition Metal Complexes. *Coord. Chem. Rev.* **2000**, *203*, 5–80.

(93) McWilliams, S. F.; Bunting, P. C.; Kathiresan, V.; Mercado, B. Q.; Hoffman, B. M.; Long, J. R.; Holland, P. L. Isolation and Characterization of a High-Spin Mixed-Valent Iron Dinitrogen Complex. *Chem. Commun.* **2018**, *54*, 13339–13342.

(94) Kandler, H.; Gauss, C.; Bidell, W.; Rosenberger, S.; Burgi, T.; Eremenko, I. L.; Veghini, D.; Orama, O.; Burger, P.; Berke, H. The Reduction of [Fe(CO)₂L₂X₂] (L = P(OMe)₃, P(OiPr)₃, PEt₃; X = Br, I) From Iron(II) to Iron(0) via Stable Iron(I) Intermediates. *Chem.—Eur. J.* **1995**, *1*, 541–548.

(95) Silantyev, G. A.; Förster, M.; Schluschaß, B.; Abbenseth, J.; Würtele, C.; Volkmann, C.; Holthausen, M. C.; Schneider, S. Dinitrogen Splitting Coupled to Protonation. *Angew. Chem., Int. Ed.* **2017**, *56*, 5872–5876.

(96) Weber, J. E.; Hasanayn, F.; Fataftah, M.; Mercado, B. Q.; Crabtree, R. H.; Holland, P. L. Electronic and Spin-State Effects on Dinitrogen Splitting to Nitrides in a Rhenium Pincer System. *Inorg. Chem.* **2021**, *60*, 6115–6124.

(97) Mercer, M.; Crabtree, R. H.; Richards, R. L. A μ -Dinitrogen Complex with a Long N–N Bond. X-Ray Crystal Structure of [(PMe₂Ph)₄CiReN₂MoCl₄(OMe)]. *J. Chem. Soc., Chem. Commun.* **1973**, 808–809.

(98) Mizobe, Y.; Yokobayashi, Y.; Oshita, H.; Takahashi, T.; Hidai, M. Preparation of Heterobimetallic Complexes with a Bridging Dinitrogen Ligand, [WX(PMe₂Ph)₄(μ -N₂)MCp₂Cl] (M = Ti, X = Cl; M = Zr, and Hf, X = I), and X-Ray Structure of [Wl(PMe₂Ph)₃(Py)-(μ -N₂)ZrCp₂Cl] (Py = Pyridine). *Organometallics* **1994**, *13*, 3764–3766.

(99) Ishino, H.; Nagano, T.; Kuwata, S.; Yokobayashi, Y.; Ishii, Y.; Hidai, M.; Mizobe, Y. Syntheses, Structures, and Reactivities of Heterobimetallic Bridging Dinitrogen Complexes Containing Group 6 and Group 4 or 5 Transition Metals. *Organometallics* **2001**, *20*, 188–198.

(100) Geri, J. B.; Shanahan, J. P.; Szymczak, N. K. Testing the Push-Pull Hypothesis: Lewis Acid Augmented N₂ Activation at Iron. *J. Am. Chem. Soc.* **2017**, *139*, 5952–5956.

(101) Specklin, D.; Coffinet, A.; Vendier, L.; del Rosal, I.; Dinoi, C.; Simonneau, A. Synthesis, Characterization, and Comparative Theoretical Investigation of Dinitrogen-Bridged Group 6-Gold Heterobimetallic Complexes. *Inorg. Chem.* **2021**, *60*, 5545–5562.

(102) Le Dé, Q.; Orbay, F.; Vendier, L.; Simonneau, A. Syntheses of N₂-bridged heterobimetallic complexes, their structural and qualitative bonding analyses. *J. Organomet. Chem.* **2023**, *986*, 122604.

(103) Peters, J. C.; Cherry, J. P. F.; Thomas, J. C.; Baraldo, L.; Mindiola, D. J.; Davis, W. M.; Cummins, C. C. Redox-Catalyzed Binding of Dinitrogen by Molybdenum N-Tert Hydrocarbylanilide Complexes: Implications for Dinitrogen Functionalization and Reductive Cleavage. *J. Am. Chem. Soc.* **1999**, *121*, 10053–10067.

(104) Assuming each set of three amido ligands donates 9 electrons to each metal in [5-MoTi](μ -N₂), the Lewis structure Mo≡N–N≡Ti that has no formal charges yields VEC = 19 e[−] on Mo and VEC = 17 e[−] on Ti; both VECs change to 18 e[−] when the charges are added to the Lewis structure.

(105) Vol'pin, M. E.; Shur, V. B. Nitrogen Fixation by Transition Metal Complexes. *Nature* **1966**, *209*, 1236.

(106) Pool, J. A.; Lobkovsky, E.; Chirik, P. J. Hydrogenation and Cleavage of Dinitrogen to Ammonia with a Zirconium Complex. *Nature* **2004**, *427*, 527–530.

(107) Pool, J. A.; Chirik, P. J. The importance of cyclopentadienyl substituent effects in group 4 metallocene dinitrogen chemistry. *Can. J. Chem.* **2005**, *83*, 286–295.

(108) Chirik, P. J. Group 4 Transition Metal Sandwich Complexes: Still Fresh after Almost 60 Years. *Organometallics* **2010**, *29*, 1500–1517.

(109) Green, J. C. Bent metallocenes revisited. *Chem. Soc. Rev.* **1998**, *27*, 263–271.

(110) Sanner, R. D.; Duggan, D. M.; McKenzie, T. C.; Marsh, R. E.; Bercaw, J. E. Structure and Magnetism of μ -Dinitrogen-Bis(Bis(Pentamethylcyclopentadienyl)Titanium(II)), {(η^5 -C₅(CH₃)₅Ti)₂N₂}. *J. Am. Chem. Soc.* **1976**, *98*, 8358–8365.

(111) Sanner, R. D.; Manriquez, J. M.; Marsh, R. E.; Bercaw, J. E. Structure of μ -Dinitrogen-bis(bis(pentamethylcyclopentadienyl)-dinitrogenzirconium(II)), {(μ^5 -C₅(CH₃)₅ZrN₂)₂N₂}. *J. Am. Chem. Soc.* **1976**, *98*, 8351–8357.

(112) de Wolf, J. M.; Blaauw, R.; Meetsma, A.; Teuben, J. H.; Gyepes, R.; Varga, V.; Mach, K.; Veldman, N.; Spek, A. L. Bis-(Tetramethylcyclopentadienyl)Titanium Chemistry. Molecular Structures of [(C₅HMe₄)(μ - η^1 : η^5 -C₅Me₄)Ti]₂ and [(C₅HMe₄)₂Ti]₂N₂. *Organometallics* **1996**, *15*, 4977–4983.

(113) While this paper was in review, Simonneau and co-workers reported the heterobimetallic complexes Cl(depe)₂Mo(μ -N₂)NbCl₄(THF) (A), Cl(depe)₂Mo(μ -N₂)TaCl₄(THF) (B), and Cl(depe)₂Mo(μ -N₂)ZrClCp₂ (C); (ref 102). The π -MoNNM configuration in A and B is isoelectronic with [5-MoTi](μ -N₂). Accordingly, the π -MO diagram predicts the Lewis structure Cl(depe)₂Mo⁺≡N–N≡M[−]Cl₄(THF). In complex C, however, the d¹-zirconocene fragment offers only one orbital of π symmetry to the MoNNZr π -system due to Cp₂M π -bonding. Thus there are only 7 π -AOs in the MoNNZr core and 3 filled π -bonding MOs; the remaining two d π electrons in MoNNZr occupy a formally nonbonding (MoNN) orbital. The total π -bond order is therefore 3, and the MO based Lewis structure is Mo=N=N=Zr with no charges, not Mo⁺≡N–N≡Zr[−]. This also corresponds to an 18-electron configuration at each metal. The significance of the difference between the derived Lewis structures is highlighted by the N–N distances in complexes A and B, 1.254 and 1.258 Å, respectively, whereas the N–N distance is significantly shorter in C, at 1.208 Å.

(114) Chatt, J.; Fay, R. C.; Richards, R. L. Preparation and Characterization of the Dinuclear Dinitrogen Complex, Trichloro- μ -Dinitrogen-Bis(Tetrahydrofuran){chlorotetrakis[Dimethyl-(Phenyl)-Phosphine]Rhenium(I)}chromium(III). *J. Chem. Soc. A* **1971**, *0*, 702–704.

(115) Doyle, L. R.; Wooles, A. J.; Jenkins, L. C.; Tuna, F.; McInnes, E. J. L.; Liddle, S. T. Catalytic Dinitrogen Reduction to Ammonia at a Triamidoamine-Titanium Complex. *Angew. Chem., Int. Ed.* **2018**, *57*, 6314–6318.

(116) Ferguson, R.; Solari, E.; Floriani, C.; Osella, D.; Ravera, M.; Re, N.; Chiesi-Villa, A.; Rizzoli, C. Stepwise Reduction of Dinitrogen Occurring on a Divanadium Model Compound: A Synthetic, Structural, Magnetic, Electrochemical, and Theoretical Investigation on the [VNNV]ⁿ⁺ [n = 4–6] Based Complexes. *J. Am. Chem. Soc.* **1997**, *119*, 10104–10115.

(117) Bezdek, M. J.; Guo, S.; Chirik, P. J. Terpyridine Molybdenum Dinitrogen Chemistry: Synthesis of Dinitrogen Complexes That Vary by Five Oxidation States. *Inorg. Chem.* **2016**, *55*, 3117–3127.

(118) Neese, F.; Atanasov, M.; Bistoni, G.; Maganas, D.; Ye, S. Chemistry and Quantum Mechanics in 2019: Give Us Insight *and* Numbers. *J. Am. Chem. Soc.* **2019**, *141*, 2814–2824.